

RXTE MEASUREMENT OF THE DIFFUSE X-RAY EMISSION FROM THE GALACTIC RIDGE: IMPLICATIONS FOR THE ENERGETICS OF THE INTERSTELLAR MEDIUM

Azita Valinia¹ and Francis E. Marshall²

Laboratory for High Energy Astrophysics

Code 662, NASA/Goddard Space Flight Center, Greenbelt, MD 20771

Accepted for Publication in the Astrophysical Journal

ABSTRACT

The diffuse X-ray emission from the thin disk surrounding the Galactic mid-plane (the so-called Galactic ridge) was measured with *RXTE* PCA in order to determine the spatial extent, spectral nature, and origin of the emission. Spatial examination of the diffuse emission in the central 30° of the plane in Galactic longitude reveals the presence of two components: a thin disk of full width $\lesssim 0.5^\circ$ centered roughly on the Galactic mid-plane, and a broad component which can be approximated as a Gaussian distribution with FWHM of about 4° . Assuming an average distance of 16 kpc to the edge of the galaxy, a scale height of about 70 pc and 500 pc is derived for the thin and broad disk components, respectively. Spectral examination of the emission clearly reveals the presence of a hard power law tail above 10 keV and an emission line from He-like iron, indicating both thermal and possibly non-thermal origins for the diffuse emission. The averaged spectrum from the ridge in the 3–35 keV band can be modelled with a Raymond-Smith plasma component of temperature $\sim 2-3$ keV and a power law component of photon index ~ 1.8 . Based on this finding, we argue that the temperature of the hot phase of the Interstellar Medium (ISM) is less than the previously reported values of 5 – 15 keV.

Motivated by the similarities between the characteristics of the thermal component of the Galactic ridge emission in our model and the thermal emission from supernova remnants (SNRs), we discuss the origin of the thermal emission in terms of a population of SNRs residing in the Galactic disk. We find that a

¹NAS/NRC Research Associate; valinia@milkyway.gsfc.nasa.gov

²marshall@milkyway.gsfc.nasa.gov

SN explosion rate of less than 5 per century is adequate to power the thermal emission from the ridge. The origin of the emission in the hard X-ray band modelled by a power law remains uncertain. Possible contributions from non-thermal bremsstrahlung of cosmic ray electrons and protons, inverse Compton scattering of energetic electrons from ambient microwave, infrared, and optical photons, non-thermal emission from SNRs, and emission from discrete X-ray sources are discussed. We speculate that bremsstrahlung of accelerated electrons and protons in SNR sites can play a significant role in producing the hard tail of the spectrum. Moreover, their collisional losses can play a major role in the ionization of the ISM.

Subject headings: galaxies: individual (Milky Way) — ISM: structure — supernova remnants — X-rays: ISM

1. INTRODUCTION

A galaxy can be well described by an ecosystem. There is an intimate relationship, much like a symbiosis, between the discrete components of the galaxy such as stars, and its interstellar medium (ISM). The ISM provides the foundation for the birth of a new generation of stars, while at the same time it is enriched by the remains of the older generations and their byproducts during their life cycle. Hence, it is natural to expect that the understanding of formation and evolution of galaxies is closely related to the understanding of their ISM.

The ISM of the Milky Way has been found to have many components. Magnetic fields and cosmic ray gas compose the relativistic fluid, while the gaseous phase consists of both ionized and neutral components. The hot ionized medium observable in UV and X-ray has a temperature above $\sim 10^5$ K and is composed of hot coronal gas heated by supernova shocks. A good portion of the energy of the ISM resides in this component. The warm ionized medium (e.g. HII, planetary nebulae) is visible in H α , UV, and optical, and has a temperature as high as 10^4 K. The neutral atomic gas appears to have both cold (< 100 K; e.g. HI clouds) and warm ($100 \text{ K} < T < 8000 \text{ K}$) components. Molecular clouds compose the self-gravitating gaseous phase. Finally the ISM (with the exception of its hot phase) is filled with dust, particles typically a few tenth of microns in size and visible through their infrared radiation. Since the peak emission of each component arises in different wavebands, multi-wavelength observations from radio to γ -rays are needed to probe the ISM.

Diffuse X-ray emission from our galaxy is a powerful diagnostic of the hot phase of the ISM. It is our purpose here to use this tool to probe the processes that contribute to its energetics and dynamics. The first detection of the X-ray emission from the Galactic disk was achieved by the pioneering rocket experiment of Bleach et al. (1972). They detected excess emission associated with a narrow disk component of angular size $2^\circ - 7^\circ$. Since then, X-ray emission from the Galactic plane and in particular the ridge (the narrow region centered on the Galactic mid-plane extending approximately to $\pm 60^\circ$ in longitude and $\pm 10^\circ$ in latitude) has been measured in the past with several satellites (e.g. *HEAO-1* [2-50 keV]: Worrall et al. 1982; *EXOSAT* [2-6 keV]: Warwick et al. 1985; *Tenma* [2-11 keV]: Koyama et al. 1986; *Ginga* [2-16 keV]: Yamasaki et al. 1997; *ASCA* [0.5-10 keV]: Kaneda et al. 1997). The presence of the 6.7 keV iron line in the spectrum discovered with *Tenma* has motivated the idea that part of the emission below 10 keV is due to a hot optically thin plasma of temperature 5 – 15 keV. Because of its high spectral resolution, *ASCA* has provided the most accurate measurement of the spectrum of the emission to date. The presence of Mg, Si, and Fe K-lines in the spectrum obtained by *ASCA* suggests that at least part of the emission is of thermal origin. Close examination of *ASCA* data has also revealed that unresolved, discrete sources are not responsible for the bulk of the emission (Yamauchi et al. 1996; Kaneda 1997). The most

recent investigation of the diffuse emission from the Scutum arm region with *ASCA* (Kaneda et al. 1997) has concluded that the emission below 10 keV has both soft ($kT \sim 0.8$ keV) and hard ($kT \sim 7$ keV) thermal components. If indeed the super hot gas (~ 7 keV) exists in an extended form in the ISM, it is not clear how to explain its confinement to the Galactic disk since its temperature exceeds the gravitational potential of the disk by at least an order of magnitude (Townes 1989). Unfortunately, the two-temperature model does not produce a good fit to the data above 10 keV indicating the presence of additional component(s) at higher energies. Indeed, a hard power law tail has been detected in the hard X-ray/soft γ -ray band from observations of the ridge with *Ginga* and the balloon experiment *Welcome-1* (Yamasaki et al. 1997), and *OSSE* (Skibo et al. 1997).

In this paper, we present the results from *RXTE* measurement of the diffuse X-ray emission from the Galactic ridge in the 3-35 keV band. Observations in the hard X-ray/soft γ -ray band have usually been complicated by the presence of numerous variable discrete sources, and the fact that the instruments generally have large fields of view and no imaging capabilities, or have imaging capability but no diffuse emission sensitivity. The combination of these factors makes the separation of emission between diffuse and compact sources a difficult task. The advantage of *RXTE* over previous missions is its small field of view (1° FWHM) combined with its wide energy bandpass (2-60 keV for the PCA), allowing for the subtraction of the contribution of discrete sources from the diffuse emission spectrum in the hard X-ray band. In addition to reporting on the detection of a hard power law tail in the *RXTE* data, we also offer an alternative interpretation for the origin of the emission below 10 keV (i.e. instead of a super hot plasma of temperature 5 – 15 keV). In agreement with previous studies, our results indicate that the emission is most likely of diffuse origin as opposed to the superposition of discrete sources. However, we present a model in which the X-ray emission is the superposition of both thermal (modelled by a Raymond-Smith plasma) and possibly non-thermal (modelled by a power law) components. We discuss the origin of the thermal component in terms of a population of SNRs residing in the disk. The origin of the power law component remains uncertain. By comparing the spectrum of the diffuse emission in hard X-rays (*RXTE*) and soft γ -rays (*OSSE*), we find indications that the emission in the two bands are related. We discuss its origin in terms of both discrete hard X-ray sources and radiation mechanisms such as non-thermal bremsstrahlung from cosmic ray electrons and protons, and inverse Compton scattering.

The plan of this paper is as follows. In §2, we describe the observations. In §3, we present the results of our spatial and spectral analysis of the data. §4 is devoted to the discussion of the results, and their implications for the origin of the emission. Finally in §5, we present our conclusions.

2. OBSERVATIONS

The Galactic ridge observations were performed in September of 1996, with the PCA instrument onboard the *RXTE* satellite. The PCA (Jahoda et al. 1996) has a total collecting area of 6500 cm², an energy range of 2 – 60 keV, and energy resolution of $\sim 18\%$ at 6 keV. The collimator field of view is approximately circular (2° diameter) with FWHM of 1° .

The observations consist of 14 long scans (from 56° to -44° in Galactic longitude) parallel to the Galactic plane up to $\pm 1.5^\circ$ and separated by 0.25° in Galactic latitude. The Galactic mid-plane (i.e. $b = 0^\circ$) was scanned twice. Fourteen shorter scans at higher latitudes parallel to the plane ($-15^\circ < l < 15^\circ$; $-4^\circ < b < -1.5^\circ$ and $1.5^\circ < b < 4^\circ$) were also performed. The speed of scans ranged from $\sim 0.6^\circ$ per minute for the shorter scans to $\sim 1.7^\circ$ per minute for the longer ones.

We constructed maps of the Galactic ridge X-ray emission from these scans in 3 energy bands. The results are shown in Figure 1. After subtraction of the instrument background (described in § 3.2), the net counts were binned into $0.25^\circ \times 0.25^\circ$ pixels for the long scans ($b \leq |1.5^\circ|$) and $0.25^\circ \times 0.36^\circ$ pixels for the shorter ones. The bins were then normalized according to exposure time. The net results are reported as count rates (cts s⁻¹) in each pixel. To smooth the images, we have interpolated them using IDL (Interactive Data Language). Since the pixel size for the long and short scans were different, each image was broken into 3 pieces: one consisting of long scans, and two others consisting of short scans at larger positive and negative latitudes. Each piece was then interpolated separately. Some of the scans at larger $|b|$ were occulted by the Earth. Therefore, we have only shown regions that were devoid of data gaps and could be smoothly interpolated. In order to emphasize the Galactic ridge diffuse emission in the images, we have used a color table that saturates the emission from discrete sources. Furthermore, we did not attempt to de-convolve the detector’s response function with the light curves. As a result, discrete sources appear as brown extended regions. For the first time, it is clear from these maps that the longitude extent of the diffuse emission in the hard X-ray band (above 10 keV) is similar to that in the softer 2-10 keV band.

3. ANALYSIS AND RESULTS

3.1. Subtraction of the Contribution of Point Sources from the Diffuse Emission Spectrum

To measure the spectrum of the diffuse X-ray emission from the Galactic ridge, we must first identify and exclude the contribution of compact sources within the paths of the scans. This task was done by an automatic routine which identifies sources with a minimum detection of 3σ . The location of each source was calculated and compared with a catalogue of known X-ray sources. The time interval in which each source was within the field of view of PCA was then excluded. Finally, the remaining good time intervals were inspected manually for detection of possible new sources. A detection of at least 10 ct s^{-1} ($\approx 1 \text{ mcrab}$) above background was interpreted as a discrete X-ray source and the time interval corresponding to the excess counts above background was excluded. From hereafter, these sources are excluded in the analysis reported in this paper. Table 1 lists all the identified sources and their positions which lied in the path of the scans. The faintest detected source in the scans has an intensity of $\sim 1 \text{ mcrab}$.

3.2. Background Subtraction

We used the PCA background estimator program *pcabackest* (version 1.4h) provided by the *RXTE* GOF (Guest Observer Facility) to estimate the background. The total background consists of the instrument background and the cosmic X-ray background (CXB). Variations in the instrument background are modelled as two components. One component is related to changes in the anti-coincidence rate, while the other is related to the activation by the SAA (Southern Atlantic Anomaly) passages. Our Galactic ridge scans were performed during non-SAA orbits and therefore the activation induced background was estimated to be zero by *pcabackest*. For modeling the latitude distribution of the diffuse emission (§3.3), we subtracted the instrument background only. For spectral analysis of the diffuse emission (§3.4), we have subtracted both the instrument and the cosmic X-ray background. Since Galactic absorption distorts the CXB spectrum at lower energies, this will result in an underestimate of the Galactic ridge flux at energies below $\sim 5 \text{ keV}$. We describe how we correct the spectrum for this effect in §3.4.2.

3.3. Latitude Distribution of the Diffuse Emission

Before performing a spectral analysis of the diffuse emission, it is crucial to have some understanding of its spatial distribution in the Galactic plane. Determining the scale height

of the emission is particularly important for at least two reasons. Firstly, it provides important clues for the origin of the emission. For example, the scale height of the emission from inverse Compton scattering is expected to be larger than that from bremsstrahlung. This is due to the homogeneous nature of the cosmic microwave background radiation and the large scale height of the optical and infrared photons and cosmic ray electrons. Secondly, it reveals the multi-component nature of the emission. For example, it can be determined whether the emission is confined to a narrow disk centered on the Galactic mid-plane or whether a broad halo around the disk also contributes to the diffuse emission.

In order to quantify the latitude distribution of the diffuse emission shown in Figure 1, we convolve the detector’s response function with a given spatial model and perform a least squared fit to the data. In Figure 2a, we have plotted the averaged diffuse emission count rate in the 5-8 keV and 8-35 keV energy bands vs. Galactic latitude. The count rate is obtained by averaging the counts at a fixed latitude over the central 30° of the Galactic plane ($-15^\circ < l < 15^\circ$) and then normalizing for exposure time. Instrumental background is subtracted. We chose the 5-8 keV energy band since above 5 keV the effects of Galactic absorption is small, and also this band implicitly maps the 6.7 keV iron line. The 8-35 keV band was chosen to map the distribution of the hard X-rays. We found that the best fit is given by a 2-component model consisting of thin and broad distributions for both energy bands. We modelled the thin component with a uniform thin disk, and the broad component with a disk of Gaussian distribution as a function of Galactic latitude. The contribution from the thin component is proportional to the distance that our line of sight traverses through the thin disk. Its value drops rapidly as $|b|$ increases, and reaches a minimum at $|b| = 90^\circ$. The contribution from the Gaussian distribution is integrated along the line of sight to the edge of the galaxy. Moreover, we added a constant component to the model to account for the cosmic X-ray background. To determine the parameters of the thin and broad components, we constrained the count rate at large Galactic latitudes to that of the cosmic X-ray background estimated from *pcabackest* and searched the parameter space for the best fit. For the 5 – 8 keV energy band, the best fit parameters are found to be $0^\circ.1^{+0.4}_{-0.06}$ for the full width of the thin component, and $4^\circ.1 \pm 0.9$ for the FWHM of the broad component at the far edge of the Galaxy ($\chi^2 = 524$, $\nu = 21$). The best fit is found when the thin component is centered at mid-Galactic plane, while the broad component is centered at $b \approx -0^\circ.12 \pm 0.15$. In Figure 2b, we have deconvolved the detector’s response function and plotted the actual contribution of each component from the model in the 5 – 8 keV band. For the 8 – 35 keV band, the best fit parameters are $0^\circ.1^{+0.3}_{-0.09}$ and $4^\circ.8^{+2.4}_{-1.0}$ for the full width of the thin component and FWHM of the broad component at the far edge of the Galaxy, respectively ($\chi^2 = 209$, $\nu = 21$). The best fit is obtained when both components are centered at $b \approx -0^\circ.03 \pm 0.15$. Error bars indicate 90% confidence limits. (Since the fits are

poor, the confidence limits are derived by setting $\Delta\chi^2 = 2.7\chi^2/\nu$.) We notice that a survey of the latitude distribution of the emission in the 50 – 600 keV with *OSSE* yields a broad distribution that is approximated with a Gaussian distribution of $5^\circ.4 \pm 0^\circ.5$ FWHM with no significant evidence of energy dependence (Purcell et al. 1996). However, in our survey, the detection of the thin disk component is statistically significant. If we fit the emission in the 8 – 35 keV band with a single Gaussian component, the χ^2 of the fit will increase from 201 (for the 2-component model) to 467. It is likely that the detection of the thin component may not be possible with *OSSE* due to its large field of view. However, we cannot determine the functional form of the thin component other than deriving limits on its width, due to the fact that the upper limit is smaller than the field of view of the PCA. As for the broad component, we point out that it is most likely related to the one reported by Iwan et al. (1982) from the measurements taken with the *HEAO* A-2 instrument. The scale height of the diffuse emission from that study was determined to be greater than 1.5 kpc.

From the reduced χ^2 reported above, it is clear that the fits are poor. This is partly the result of the asymmetry of the overall profile of the diffuse emission with respect to the Galactic mid-plane. From Figure 2a, it also appears that at some latitudes the count rates substantially deviate from that of the model. We have inspected the source excluded data, but they do not appear to be contaminated with any sources above our detection level. Hence, we conclude that additional spatial components at certain latitudes corresponding to localized features of the diffuse emission are needed to produce a better fit. However, the derived parameters provide a good global description of the spatial distribution of the diffuse emission in the Galactic plane.

3.4. Diffuse Emission Spectrum and its Variation as a Function of Galactic Latitude

To determine the spectral variation of the diffuse emission from the Galactic ridge as a function of Galactic latitude, we performed separate spectral analysis on the data from the central ridge (R1), the northern ridge (R2), and the southern ridge (R3). The coordinates of each region are given in Table 2. We will discuss the results of spectral fitting for the central ridge first. Spectral analysis for regions R2 and R3 will be presented in §3.4.3.

3.4.1. Central Ridge Spectrum in the 10 – 35 keV band

Since Galactic disk absorption distorts the spectrum of both the Galactic ridge emission and the cosmic X-ray background (CXB) at lower energies, we analyse the data above 10 keV first, where absorption is negligible for the expected Galactic column densities. This strategy will allow us to constrain the component(s) that dominate the spectrum in the hard X-ray band. We will then use this derived information to model the spectrum at lower energies.

The presence of a hard power law tail above 10 keV has been reported from combined observations with *Ginga* and *Welcome-1* (Yamasaki et al. 1997) and *OSSE* (Skibo et al. 1997). Here, we search for this component by fitting the *RXTE* data in the 10 – 35 keV energy range with a single power law component. The best fit yields a photon index of $\Gamma = 2.1^{+0.2}_{-0.3}$ with a normalization of $k = 8.5^{+8.5}_{-4.0} \times 10^{-3}$ photons keV $^{-1}$ cm $^{-2}$ at 1 keV ($\chi^2/\nu = 56.5/44 = 1.3$). The surface brightness for the 10–35 keV band is 4.9×10^{-8} erg s $^{-1}$ cm $^{-2}$ sr $^{-1}$. Figure 3 shows the unfolded spectrum. A thermal bremsstrahlung for the data above 10 keV requires a temperature of 20^{+11}_{-5} keV. However, we prefer the power law model since it is not clear how the hot plasma can be bound to the Galactic disk (the gravitational potential of the disk is ~ 0.5 keV). Furthermore, the presence of the power law at soft γ -ray energies has been established with *OSSE*. It is likely that the emission in the hard X-ray and soft γ -ray both modelled by a power law are related. We will discuss this further in §3.6.

3.4.2. Central Ridge Spectrum in the 3 – 35 keV band

Let us now extend the data analysis to lower energies. Below 10 keV, the presence of a 6.7 keV emission line from He-like iron was discovered with *Tenma* (Koyama et al. 1986). Further extensive study of the ridge spectrum with the high resolution capability of *ASCA* has revealed the presence of lower energy emission lines from Mg, Si, and S (Kaneda et al. 1997). These findings have motivated the idea that part of the emission has thermal origin. Furthermore, we use the results of the previous section where the presence of a power law tail in the spectrum above 10 keV has been established. Hence, we model the data with both Raymond-Smith (RS) plasma and power law components. Notice from Figure 2 that the emission in the central ridge (R1) arises from both the thin disk and the broad components. However, since the spectral decomposition of the broad and thin components is complicated and not well constrained with current statistics, we model the averaged effect of the two components.

Before modeling the data, we should first consider the effect of Galactic disk absorption on the final spectrum. Since we have subtracted the high latitude cosmic X-ray background

from our data, the Galactic ridge flux at lower energies may have been underestimated. This is because for expected Galactic column densities, absorption reduces the CXB flux mostly below ~ 10 keV, but will leave the spectrum above 10 keV unchanged. Therefore, in order to compensate for this effect, we subtract the high latitude CXB model from our spectral model but add the absorbed CXB model (had it been absorbed by the Galactic disk). The spectrum of the CXB below 15 keV was modelled from *RXTE* high latitude observations. The spectrum was found to have a power law shape of photon index $\Gamma = 1.47$ with normalization $k = 3.6 \times 10^{-3}$ photons keV $^{-1}$ cm $^{-2}$ at 1 keV corresponding to a surface brightness of 5.7×10^{-8} erg s $^{-1}$ cm $^{-2}$ sr $^{-1}$ in the 3 – 10 keV. Notice that since *RXTE* is not designed to separate instrument background from the cosmic X-ray background, some residual counts inherent to the detectors' background may exist in the CXB model at higher energies, but its effect on our modeling is negligible. In effect, we add the term $(-kE^{-\Gamma}(1 - \exp^{-N_H\sigma(E)}))$ to our model where $kE^{-\Gamma}$ is the CXB model and N_H and $\sigma(E)$ are the Galactic column density and the photoelectric cross section as a function of energy, respectively. However, the precise value of the Galactic hydrogen column density as a function of position and its averaged effect over 90° in Galactic longitude (the span of the central ridge studied here) are not well known. Therefore, while we freeze the parameters of the CXB model in our analysis, we fit for the Galactic column density along with the rest of the model parameters. This correction is applied to all models we present hereafter.

The best fit parameters for the model described above are presented in Table 3. The data and unfolded spectrum are shown in Figure 4. From these results, on average, the emission can be explained by a Raymond-Smith plasma of temperature ~ 3 keV and a power law component with photon index $\Gamma \sim 1.8$ which dominates above 10 keV. In the 3 – 10 keV band, 54% of the flux is from the thermal Raymond-Smith plasma component. Above 10 keV, the power law component dominates by providing 95% of the flux. Confidence contours for $kT - \Gamma$ are shown in Figure 5. The average column density derived from this model is well within the expected Galactic values. It may be argued that the column density N_H absorbing the CXB component may be larger than that absorbing the RS plasma and power law components since in the case of CXB the entire material between us and the edge of the Galaxy acts as the absorber (i.e. longer path length). Had we frozen the value of the column density absorbing the CXB component at an upper limit of 3×10^{22} cm $^{-2}$, the key fit parameters would change to $N_H = 1.3_{-0.6}^{+0.8}$ cm $^{-2}$, $\Gamma = 1.85 \pm 0.15$, and $kT = 2.9_{-0.3}^{+0.4}$ keV ($\chi^2/\nu = 112.9/60 = 1.9$). These are all within the error bars of the values presented in Table 3.

We point out that these results do not indicate that the spectrum measured with *RXTE* is inconsistent with that from *ASCA*. We modeled the *RXTE* data from region R1 in the 3 – 10 keV with the same components with which *ASCA* data from the Scutum arm region

was modeled (Kaneda et al. 1997), namely 2 thermal components of temperature ~ 0.8 and ~ 7 keV, respectively. The fit was acceptable with $\chi^2/\nu = 13.5/10 = 1.35$. However, when we extend this model to higher energies, the fit is poor ($\chi^2/\nu = 141.9/58 = 2.4$). This is mainly due to the observed count rate being greater than that of the model at higher energies, and can be easily seen from Figure 6. In the case of *RXTE* analysis, the additional data at higher energies allows us to constrain the component that dominates in the hard X-ray band. This in turn, affects the results of spectral modeling at lower energies.

Finally, we present a slight variation of our model in which the power law is flattening below some energy between 10 – 100 keV. The motivation for this model is two-fold. First, unusually large power is required to be injected into the galaxy in order to explain the presence of the power law tail via non-thermal bremsstrahlung process. We will discuss the physical reasons for this in §4.2. Second, there is evidence for the flattening of the slope at lower energies (see §3.6 where we discuss simultaneous fitting of the spectrum with that from *OSSE*). But for now, we will only present the model. The attenuation of the power law can be mimicked by multiplying the power law function by an exponentially absorbing function $M(E) = \exp(-E_0/E)$. Table 4 lists the best fit parameters for this model. Figure 7 shows the model and unfolded spectrum. Approximately 58% of the flux in the 3 – 10 keV is due to the thermal component in this model.

3.4.3. Spatial Variation of the Spectrum as a Function of Galactic Latitude

Let us now examine the spectrum of the diffuse emission from the ridge at larger Galactic latitudes. From Figure 2, it can be seen that the broad spatial component dominates the emission at larger latitudes. We used the same model discussed in the previous section to fit the data for Galactic regions R2 and R3 (Table 3). The results of the fits are summarized in Tables 5 and 6, respectively. Since, the broad component is expected to be less absorbed than the thin disk component, it is reasonable that the average values of the hydrogen column density for these regions have decreased compared to that of the central ridge. The key fit parameters (namely kT of the RS component and the photon index of the power law) have remained within error bars of those derived for the central ridge indicating similar physical origins at higher latitudes. The average flux in the 3 – 35 keV band from both regions is about 82% of that from the central ridge after removing the effect of absorption.

3.5. X-ray Luminosity of the Galactic Ridge

Let us now estimate the X-ray luminosity of the diffuse emission for the Galactic disk in the 2 – 10 keV and 10 – 60 keV bands. In reality, this is a complex problem since it depends on the geometry and spatial distribution of the emitting and absorbing regions. A rigorous treatment of this problem is outside of the scope of this paper. However, we proceed to estimate the luminosity by making a few simple assumptions. From our spatial modeling of the latitude distribution of the emission (§3.3), we found that 2 spatial components (i.e. a thin disk and a broad component) contribute to the emission. Since the flux at $|b| > 1^\circ$ is dominated by the broad component (as seen from Figure 2), we will first estimate the average volume emissivity of the broad component from spectral models of regions R2 and R3. From the models presented in Tables 5 and 6, we find an average flux of $2.4 \times 10^{-11} \text{ erg s}^{-1} \text{ cm}^{-2}$ and $1.9 \times 10^{-11} \text{ erg s}^{-1} \text{ cm}^{-2}$ in the 2 – 10 keV and 10 – 60 keV bands, respectively, after removing the effect of absorption. Dividing the flux by the *effective* solid angle of *RXTE* ($2.97 \times 10^{-4} \text{ sr}$) yields an average surface brightness B of $8.1 \times 10^{-8} \text{ erg s}^{-1} \text{ cm}^{-2} \text{ sr}^{-1}$. For a spherical geometry with uniform emissivity, the average volume emissivity along the line of sight can be estimated to be $\bar{\epsilon} = B(4\pi/l)$ where l is the depth of the emitting region. This is a good approximation for the broad component. We assume that the distance to the Galactic center and the radius of the Galactic disk are 8 and 10 kpc, respectively. Choosing an average line of sight of length 16 kpc, we find the average volume emissivity $\bar{\epsilon}_{\text{broad}}$ to be $2.1 \times 10^{-29} \text{ erg s}^{-1} \text{ cm}^{-3}$. The FWHM of the broad component is about 4° corresponding to a disk of height $\sim 1 \text{ kpc}$. This yields $1.8 \times 10^{38} \text{ erg s}^{-1}$ for the the X-ray luminosity of the broad disk. From our spatial model presented in §3.3, the ratio of the luminosity of the broad to the thin disk is about 14. The total luminosity of the disk (thin plus broad) in this model is then estimated to be $\sim 2 \times 10^{38} \text{ erg s}^{-1}$ in the 2 – 10 keV band. Similarly, we derive a luminosity of $1.5 \times 10^{38} \text{ erg s}^{-1}$ in the 10 – 60 keV.

For comparison purposes, we should mention that Koyama et al. (1986) have reported a luminosity of $\sim 10^{38} \text{ erg s}^{-1}$ from observations with *Tenma* (2 – 11 keV). Worrall et al. (1982) have reported a luminosity of $1.4 \times 10^{38} \text{ erg s}^{-1}$ in the 2 – 10 keV band with HEAO-1, while Warwick et al. (1985) have reported a luminosity of $\sim 1.7 \times 10^{38} \text{ erg s}^{-1}$ with *EXOSAT* in the 2 – 6 keV band (notice that this band does not include the iron line emission). From the latest *ASCA* survey, Kaneda et al. (1997) report a luminosity of $2 \times 10^{38} \text{ erg s}^{-1}$ for the hard component in the 0.5 – 10 keV band where the hard component is modelled by a bremsstrahlung of temperature 7 keV. The effect of absorption has been taken into account in all the previously reported estimates.

3.6. Extension of the Diffuse Emission Spectrum from hard X-ray to the Soft γ -ray Band

In the previous sections, we established the presence of a hard power law tail above 10 keV. Recent diffuse emission measurement of the Galactic plane at longitude 95° with *OSSE* in the 50 – 500 keV band also reveals that the spectrum can be fitted with a power law model ($\Gamma = 2.6 \pm 0.3$; Skibo et al. [1997]). If the spectrum extends smoothly from the hard X-ray to the soft γ -ray regime, it means that the same physical processes are dominating the emission in a wide bandpass. Unfortunately *RXTE* data at Galactic longitude of 95° are not available yet. However, assuming that the spectral shape of the diffuse emission is the same as a function of galactic longitude for $|b| \leq 2^\circ$ (Purcell et al. 1996), and that only the normalization varies, we attempt a simultaneous spectral fit to the spectrum of the diffuse emission from both *RXTE* and *OSSE*. We use the *RXTE* data from the central ridge (R1) above 10 keV and simultaneously fit it with the data obtained with *OSSE* at Galactic longitude of 95° . The results of the fit appear in Figure 8. The fit yields a power law photon index of 2.3 ± 0.2 which is within the errors bars of the values derived from either *RXTE* above 10 keV ($\Gamma = 2.1^{+0.2}_{-0.3}$) or *OSSE* ($\Gamma = 2.6 \pm 0.3$) alone. The normalization for the *RXTE* and *OSSE* data are $1.5^{+1.2}_{-0.6} \times 10^{-2}$ and $0.19^{+0.32}_{-0.12}$ photons $\text{s}^{-1} \text{cm}^{-2}$ at 1 keV, respectively. The fit is acceptable with a total χ^2 of 147.6 for 118 degrees of freedom. In order to compare the normalizations of the power law component derived from *RXTE* and *OSSE*, we must calculate the flux per steradian (photons $\text{s}^{-1} \text{cm}^{-2} \text{sr}^{-1}$) for each instrument. However, for extended emission, the measured flux depends on the field of view of each instrument and the distribution function of the diffuse emission. Hence, an *effective* solid angle (i.e. the convolution of the distribution of the emission with the detector's response function) should be calculated for each instrument. In the case of *OSSE* (fov of 11.4×3.8 FWHM), convolving the soft γ -ray Galactic diffuse emission (assuming a Gaussian distribution with $\sim 5^\circ$ FWHM [Purcell et al. 1996]), and *OSSE*'s triangular response function yields an *effective* solid angle of $\sim 1.3 \times 10^{-2}$ sr. Similarly *RXTE*'s solid angle is $\sim 3 \times 10^{-4}$ sr. Therefore, the normalization parameter for the power law component from *OSSE* should be multiplied by 2.3×10^{-2} to be compared with the normalization derived from *RXTE*. This yields a normalization of 4.4×10^{-3} photons $\text{keV}^{-1} \text{cm}^{-2} \text{s}^{-1}$ at 1 keV for the power law component measured with *OSSE*, which is a factor of 3.4 smaller than the normalization of the power law component from *RXTE* data. This is expected since the intensity of the emission seen with *RXTE* decreases away from the Galactic center.

If we assume that the physical origin of the power law is the same for the averaged central ridge and at Galactic longitude 95° , then the combined *RXTE/OSSE* fit gives a narrower constraint on the power law slope. However, the slope at higher energies is noticeably steeper than that derived for the spectrum below 35 keV, perhaps hinting that the power law either

flattens or slowly attenuates at lower energies.

4. DISCUSSION: IMPLICATIONS FOR THE ORIGIN OF THE EMISSION

4.1. Discrete Sources

We first consider the contribution of unresolved discrete sources to the diffuse emission spectrum. The important question is whether there exist classes of unresolved discrete sources with appropriate spatial number densities and similar spectra to that of the diffuse emission that can comprise the bulk of the spectrum.

In the hard X-ray band (above 10 keV), the number of known Galactic hard X-ray sources with similar spectra to that of the Galactic ridge diffuse emission is small (Levine et al. 1984). Black hole candidates in their soft state have spectra similar to that of the ridge, but this is usually seen at high luminosities when individual sources can be easily detected. Neutron star binaries are known to have hard power law spectra with an exponential cut off around 20 keV. However, only a handful of them are known to be active at a time in the Galactic disk. Also, their luminosities are mostly in the range $10^{36} - 10^{38} \text{ erg s}^{-1}$ which can easily be detected from the diffuse emission. Unresolved pulsars are also thought to contribute to the Galactic ridge diffuse emission particularly in the γ -ray band. A recent study, however, concludes that pulsar contribution to the diffuse Galactic emission is significant only above 1 GeV (Pohl et al. 1997).

In the soft γ -ray band, simultaneous *SIGMA*/*OSSE* observations of the Galactic center region has been performed to distinguish the diffuse emission from that of compact sources (Purcell et al. 1996). Comparison of the source excluded spectrum from the Galactic center and that from regions which are known to have fewer sources (i.e. $l = 25^\circ$ and 339°) has revealed that the spectra are similar in both intensity and spectral index. If the emission is due to discrete sources, 10 X-ray sources of flux $\leq 5 \times 10^{-3} \text{ photons cm}^{-2} \text{ s}^{-1} \text{ MeV}^{-1}$ at 100 keV must be present in the field of view of *OSSE* to make up the spectrum. Because of the lack of knowledge of such class of sources with a uniform space density in longitude, it is likely that the emission above 10 keV is of diffuse origin.

Below 10 keV, because of its better spatial resolution, *ASCA* is far better equipped than *RXTE* to resolve individual faint sources. A recent fluctuation analysis of the surface brightness of the ridge emission in the Scutum arm region ($l = 28^\circ.5$, $b = 0^\circ$) with *ASCA* has concluded that if discrete sources are to make up the entire spectrum, their luminosity must be less than $2 \times 10^{33} \text{ ergs s}^{-1}$ (Yamauchi et al. 1996). This conclusion narrows the field of candidate class of sources that can make up the diffuse emission spectrum of the Galactic

ridge. Among possible class of sources, neutron stars (with X-ray luminosities mostly in the range $10^{36} - 10^{38} \text{ erg s}^{-1}$) are unlikely due to their large luminosities. A likely class of sources that has been thought to account for the emission is the RS CVn type binaries, since they exhibit the iron K line in their emission spectra. However, a study by Ottmann & Schmitt (1992) on the contribution of RS CVn systems to the Galactic diffuse emission concludes that while they contribute about 6% to the total Galactic background, their contribution to the Galactic ridge iron line is too small ($\sim 1\%$). Therefore, given the strength of the iron line in the spectrum of the diffuse emission, it seems that unresolved RS CVn sources do not contribute to the bulk of the emission. Cataclysmic Variables (CVs) are another candidate that may contribute to the Galactic ridge diffuse emission. They have similar spectra to that of the ridge and their luminosities fall in the range $10^{31} - 10^{33} \text{ erg s}^{-1}$. However, from the analysis of the *ASCA* GIS pointings of the Galactic ridge, Kaneda (1997) has shown that in order for CVs to make up the diffuse emission, their space densities would have to be $\sim 7 \times 10^{-4} \text{ pc}^{-3}$, a factor of 100 larger than the estimated density of CVs (Patterson 1984).

For these reasons, it is more likely that the emission is due to diffuse or extended sources. A more detailed review of the previous works on the contribution of the discrete sources to the ridge spectrum can be found in Kaneda (1997) and Yamasaki (1996), and references therein. Finally, we point out that with the upcoming launch of *AXAF*, a more sensitive number-flux distribution of Galactic sources and their exact contribution to the diffuse Galactic background can be determined.

4.2. Diffuse Emission

Based on our measurements presented in this paper, we conclude that the diffuse emission from the ridge in the broad X-ray and soft γ -ray band has both thermal and possibly non-thermal origins. In what follows, we speculate on the origin of the emission, first focusing on the thermal component and then speculating on the origin of the power law tail.

The thermal component can be modelled with a Raymond-Smith plasma of temperature $\sim 2 - 3 \text{ keV}$ (Tables 3 and 4). However, we point out that the spectral resolution of *ASCA* GIS or SIS is far superior to that of *RXTE* PCA. Therefore, in order to interpret the spectrum accurately, we need to carefully examine the spectral features of the diffuse emission below 10 keV using the *ASCA* data. For this reason, we refer to the latest investigation of the diffuse emission from the Galactic ridge with *ASCA* (Kaneda 1997; Kaneda et al. 1997). The spectral examination of the *ASCA* data has clearly verified the presence of lower energy emission lines from Mg, Si, and S. The spectrum has also been carefully examined for the presence of Fe K lines. While the emission line from He-like iron was clearly detected, the

presence of the emission lines from neutral and H-like iron was not firmly established. This is important since the equivalent width of the H-like iron line sets an upper limit for the plasma temperature. Kaneda et al. (1997) give an upper limit of $\sim 1/6$ of that of the He-like iron for the normalization of the H-like iron line. This implies an upper limit of $4 - 5$ keV for the plasma temperature. This is in agreement with our results since the emission line from H-like Fe is expected to be very weak from a $2 - 3$ keV plasma, supporting our finding that the thermal component of the emission arises from a gas of cooler temperature. Therefore, we argue that unlike previous conclusions (Koyama et al. 1986; Kaneda et al. 1997), the temperature of the X-ray emitting gas need not be so high ($5-15$ keV) in order to produce the observed spectrum. This interpretation lessens the difficulties toward explaining the origin and confinement of the super hot (> 5 keV) gas.

Due to the similarities between the characteristics of supernova remnants and the thermal nature of the diffuse emission spectrum presented here, we speculate that a collection of supernova remnants in the galactic disk, below current X-ray and/or radio detection limits, is responsible for the thermal origin of the diffuse emission. The idea was originally introduced by Koyama, Ikeuchi, & Tomisaka (1986, hereafter KIT86). However, in their calculation, they assumed that the temperature of the emitting gas is about ~ 7 keV. In addition to the fact that no SNR with such high temperature has ever been detected, this assumption also requires a large SN explosion rate (one per 10 years) which exceeds the expected Galactic rate of 2-3 per century (Tammann 1982). Below, we revisit their argument in order to derive the SN explosion rate capable of powering the thermal emission from the ridge using the adjusted temperature of $2 - 3$ keV for the emitting plasma.

The first step is to estimate the criteria for which a given SNR is below radio detection limit. Due to absorption in the Galactic disk, the minimum radio surface brightness for detecting a SNR is $10^{-20} \text{ W m}^{-2} \text{ Hz}^{-1} \text{ sr}^{-1}$. Using the empirical relation between the surface brightness Σ , and the diameter of the SNR (Milne 1979), and accounting for the ambient gas density as a function of scale height of the Galactic plane (Tomisaka, Habe, & Ikeuchi 1980), KIT86 reduce the criteria to

$$\Sigma = \Sigma_0 D^{-3.8} n_a^2 < 10^{-20} \text{ W m}^{-2} \text{ Hz}^{-1} \text{ sr}^{-1}, \quad (1)$$

where $\Sigma_0 = 2.88 \times 10^{-14} \text{ W m}^{-2} \text{ Hz}^{-1} \text{ sr}^{-1}$, and

$$D = 2R_s = 2(0.31 n_a^{-0.2} E_{51}^{0.2} t^{0.4}) \text{ pc}, \quad (2)$$

where R_s is the radius of the SNR in the adiabatic stage described by the similarity solution (Sedov 1959; Spitzer 1968), and t , E_{51} and n_a are the age (years), total energy of the SNR (in units of 10^{51} erg), and the density of the ambient medium (cm^{-3}), respectively. Substitution

of equation (2) in equation (1) yields

$$n_a t_3^{-0.55} < 0.11 E_{51}^{0.28}, \quad (3)$$

where $t_3 = t/10^3$.

Assuming that the thickness of the emitting region at the shock is $\sim R_s/12$, the X-ray luminosity of the blast wave shell can be calculated from

$$L_X = (\pi/3) \varepsilon R_s^3, \quad (4)$$

where R_s is described by equation (2) and ε is the total emissivity of the gas and depends on the electron density n_e and the cooling function Λ via the relation $\varepsilon = n_e^2 \Lambda(T)$. For a strong shock $n_e \simeq 4n_a$. The cooling function $\Lambda(T)$ is estimated to be (Raymond, Cox, & Smith 1976)

$$\Lambda(T) = 2.2 \times 10^{-19} T^{-0.6}, \quad (5)$$

for a gas of $10^5 \text{ K} < T < 4 \times 10^7 \text{ K}$ ($0.008 \text{ keV} < T < 3.3 \text{ keV}$). In Figure 9, we have plotted the condition for the undetectability of a SNR in the radio band (eq. [1]), and the restriction on the temperature of the blast wave ($2 \text{ keV} < kT < 3 \text{ keV}$) in the $n_a - t$ phase space where the temperature just behind the shock front can be calculated from $T = (3\mu/16k)(dR_s/dt)^2$ and μ and k are the mean mass of the gas particle and the Boltzman constant, respectively. We have also plotted relevant constant luminosity lines. From the region of the allowed parameters in this plot, we conclude that the average luminosity and age of the contributing SNRs is expected to be $\sim 5 \times 10^{35} - 10^{36} \text{ erg s}^{-1}$ and $(4 - 5) \times 10^3$ years, respectively. The X-ray luminosity of the entire disk in the $2 - 10 \text{ keV}$ band from the *thermal* component (which accounts for approximately 50% of the emission) is estimated to be $\sim 10^{38} \text{ erg s}^{-1}$ (§3.4.2). This implies that a SN explosion rate of $\sim 3 - 5$ per century is required to power the thermal emission from the entire disk. On the other hand, the luminosity of the thermal component of the thin disk is about $6 \times 10^{36} \text{ erg s}^{-1}$. Then a SN explosion rate of ~ 1 per century is sufficient to power the thermal emission from the thin disk.

Whether this scenario is viable depends on the number of SNRs that are actually detected in the X-ray band in the Galactic ridge. If the SNRs have an average luminosity of $5 \times 10^{35} \text{ erg s}^{-1}$, approximately 200 of them are needed to power the thermal emission from the ridge. So far, 215 SNRs have been detected in the radio band (Green 1996). Based on the prevalence of SNRs among a sample of unidentified Galactic radio sources, Helfand et al. (1989) have built a model which predicts the existence of up to ~ 590 SNRs in the Galactic disk in the radio band. According to their results, these remnants are within detection capability of current instruments but are not yet identified. One of the goals of the *ASCA* Galactic Plane Survey Project is to identify SNRs in the Galactic disk (in the region $|l| < 45^\circ$

and $|b| < 0.8^\circ$) that have already been catalogued in other wavebands, and to discover new ones. Because of Galactic absorption, remnants with low surface brightness will be missed in the survey. However, SNRs with fluxes greater than 10 Jy at 1GHz will be detected with *ASCA* provided no bright sources are in the field of view. From the most recent *ASCA* survey covering the region $l = 342^\circ - 357^\circ$ and $b = 1^\circ - 16^\circ$ pointed at $b = 0^\circ$, 13 SNR were detected (Yamauchi et al. 1998 and references therein), where 25 SNRs in radio and 1 SNR in X-ray (discovered with *ROSAT*) were already known to exist. Based on this trend, it can be estimated that approximately half of the radio SNRs have significant emission in X-ray. It may then be expected that out of the 215 SNRs catalogued in radio, approximately 100 of them should be detected in X-ray. If, we take the prediction of Helfand et al. (1989) at face value, this number increases to ~ 300 . Ultimately, whether the Galactic SNR population can power the thermal emission from the ridge depends on the final number of detected SNRs and their average luminosity when the *ASCA* survey is completed.

We now turn to the discussion of the origin of the power law tail of the spectrum dominating the hard X-ray/soft γ -ray band. Recent analysis of diffuse emission from the Galactic ridge with *ASCA* (Kaneda et al. 1997) indicates that the spectrum can be fitted with a two temperature non-equilibrium ionization plasma of $kT \sim 0.8$ and 7, respectively. Two factors lead us to believe that the reported high temperature component of 7 keV with *ASCA* is in fact a different interpretation of the power law component reported in this paper. Firstly, *ASCA*'s sensitivity above 10 keV decreases substantially and goes to zero around 12 keV. Thus, distinguishing the power law from the hard thermal component in the *ASCA* data may not be possible. Secondly, extension of the two-temperature model above 10 keV does not produce a good fit to the data at higher energies (as shown in §3.4.2). On the other hand, we have unambiguously shown here the presence of the hard power law tail in hard X-ray data. This leads us to conclude that the previously reported super hot (> 5 keV) component of the ISM, is most likely due to non-thermal emission with a power law spectrum that dominates above 10 keV and extends to beyond 100 keV. Below, we speculate on the origin of the power law tail.

One scenario is to interpret the hard X-ray emission as the result of the superposition of non-thermal tails from SNRs. Previously non-thermal X-ray emission from SN1006 (Koyama et al. 1995) and RX J1713.7-3946 (Koyama et al. 1997) has been reported. Non-thermal γ -ray emission from Cas A (The et al. 1995) and a high energy tail in its X-ray spectrum which can be possibly attributed to non-thermal processes (Allen et al. 1997) has also been discovered. However, it is not clear if this scenario can account for the bulk of the emission. The X-ray luminosity of the non-thermal emission discovered is about an order of magnitude smaller than the luminosity of the thermal component. In the case of Cas A for example (G. E. Allen, private communication), the luminosity in the 2-10 keV band is

$1.6 \times 10^{36} \text{ erg s}^{-1}$, while the luminosity in the 10-60 keV is about $2 \times 10^{35} \text{ erg s}^{-1}$. From our estimates, the luminosity of the ridge is approximately $2 \times 10^{38} \text{ erg s}^{-1}$ and $1.5 \times 10^{38} \text{ erg s}^{-1}$ in the 2-10 keV and 10-60 keV bands, respectively. The contribution of the SNRs to the thermal component of the spectrum was previously addressed in this section. For the power law tail (interpreted as non-thermal component), this suggests that approximately 750 SNRs with non-thermal luminosities of $2 \times 10^{35} \text{ erg s}^{-1}$ are needed to make up the high energy tail of the spectrum. Thus far, substantial number of remnants that exhibit non-thermal emission has not been discovered. Therefore, the viability of this scenario awaits further observations.

X-rays of 10-100 keV can also be produced via inverse Compton scattering of energetic electrons on the ambient microwave background, optical, and infrared photons. A power law scattered photon spectrum with photon index $(p + 1)/2$ is expected if the electron spectrum has energy index p . However, the exact contribution from this process is model dependent due to the uncertainty in the interstellar radiation field and the electron spectrum. Direct measurement of the electron spectrum is reliable only at GeV energies because of the effects of solar modulation at lower energies. Irrespective of existing models for the Compton scattering contribution and their extrapolation to lower energies, Skibo, Ramaty, & Purcell (1996) have argued that this mechanism does not produce the bulk of the emission below 100 keV. Since Compton scattering of microwave background and star light photons require electron energies of 100 MeV-10 GeV, the electron spectrum must turn up somewhere in that energy range. However, electrons at these energies produce the Galactic synchrotron radio emission at 100 MHz frequencies. But since the observed radio spectrum breaks at $\sim 100 \text{ MHz}$ in the opposite sense to that of the γ -ray emission, they argue that an inverse Compton origin is unlikely.

A likely possibility for the origin of the power law tail is non-thermal bremsstrahlung. However, bremsstrahlung of sub-MeV electrons is highly inefficient due to the fact that ionization and Coulomb collision losses exceed bremsstrahlung radiation. For example, for a 100 keV electron, the radiation yield (i.e. the ratio of energy loss from radiation to that from collision) is $\sim 2.5 \times 10^{-4}$ (Berger & Seltzer 1964). For a 10 keV electron, the yield drops to 3.8×10^{-5} . From our estimate, the luminosity of the ridge in the 10 – 60 keV band is $\sim 1.5 \times 10^{38} \text{ erg s}^{-1}$. An order of magnitude estimate implies that in order to account for the power law tail via electron bremsstrahlung, a power of $10^{41} - 10^{42} \text{ erg s}^{-1}$ is required. Skibo et al. (1996) have calculated that a total power input up to $\sim 10^{43} \text{ erg s}^{-1}$ is required if the tail extends down to 10 keV. The total injected power into the Galaxy via supernova explosion is only $\sim 10^{42} \text{ erg s}^{-1}$ assuming 10^{51} erg is released in a SN explosion every 30 years. Several attempts have been made to explain the source of this large power. Skibo et al. (1996) have suggested that the power is derived from the release of the gravitational potential upon the passage of ISM through galactic spiral arm compressions. Schlickeiser (1997) explains the

implied presence of large population of sub-MeV electrons with the existence of interstellar in-situ reacceleration of cosmic ray particles by the ambient interstellar plasma turbulence. Based on the empirical results of modelling the data in the wide bandpass of 3-500 keV, we suggest that the power law tail should gradually attenuate below some energy in the 10-100 keV range (Table 4). This speculation is motivated by comparing the spectral fits of the data above and below 10 keV. Above 10 keV, we found that the spectrum can be modelled with a power law of photon index 2.3 ± 0.2 up to 500 keV. On the other hand, when modelling the data in the 3 – 35 keV band, the power law slope is 1.8 ± 0.1 . This interpretation lessens the large power requirement for the origin of the power law component via bremsstrahlung and results in the required injection power to be consistent with that expected from SN explosion in the galaxy. Unfortunately, the electron spectrum cannot be measured due to solar modulation at lower energies. However, our interpretation of the data in this way makes a prediction for the shape of the electron spectrum at lower energies. A detailed calculation of the electron spectrum in this scenario is out of the scope of this paper.

In addition to electron bremsstrahlung, we suggest the possibility that *inverse* (or proton) bremsstrahlung may also contribute to the diffuse emission from the Galactic ridge. In the inverse process, the rapidly moving proton radiates instead of the electron and the center of momentum of the proton-electron system is approximately that of the moving proton. Boldt & Serlemitsos (1969) have shown that significant radiation is associated with the collisions of suprathermal protons with ambient electrons (free and bound). For the non-relativistic case ($\beta \ll 1$), the spectral intensity from the bremsstrahlung of an electron with kinetic energy E is the same as that from a suprathermal proton of kinetic energy $(M/m)E$, where m and M are the rest mass of the electron and proton, respectively. For example, an electron with kinetic energy of 10 keV produces the same spectral intensity as that of a proton with kinetic energy of 20 MeV. The scenario is particularly attractive in the context of particle acceleration and reacceleration in supernova shocks via the diffusive Fermi process. For many years, the perception has persisted that supernova remnants are a major source of Galactic cosmic rays (e.g. Lagage & Cesarsky 1983). Recently much work has been done regarding the production of γ -rays in the SNRs. Modelling of γ -ray production via interaction of the energetic particles with the remnants’ ambient environment through neutral pion decay, bremsstrahlung, and inverse Compton scattering is reviewed by Baring (1997). One expects that if both electrons and protons are accelerated with equal velocities in the explosion process, both should contribute to the bremsstrahlung emission. The ratio of the bremsstrahlung losses to the collisional losses is roughly the same for both electrons and protons since it is only dependent on the velocity of the radiating particles. However, a simple calculation shows that not only the accelerated protons’ lifetime is longer than that of electrons’, but also they travel farther than electrons from their birthplace. To illustrate this,

let us consider bremsstrahlung radiation from an electron of 25 keV. Its spectral intensity is similar to that from a proton of 50 MeV. However, the range R of the 25 keV electron in hydrogen is $5.6 \times 10^{-4} \text{ g cm}^{-2}$ as opposed to 1.0 g cm^{-2} for the 50 MeV protons (Berger & Seltzer 1964; Barkas & Berger 1964). This translates to distances of approximately 100 pc and 0.2 Mpc for the electrons and protons, respectively. The radial distance S from the birthplace of the energetic particles which the particles will travel before they lose all their energy depends on the random walk step length λ via the relation $S/\lambda = (R/\lambda)^{1/2}$. While the value of λ is not well known, it is expected to be much larger than the gyro radii of the particles for the expected Galactic magnetic fields but somewhat smaller than the height of the Galactic disk. A good estimate is that it is on the order of the coherence length of the magnetic fields. As a quantitative value for this length, we use the study of Kim, Kronberg, & Lancecker (1988) where they probed the structure of magnetic fields in and around the supernova remnant OA 184 (G166.2+2.5) using background radio source rotation measures. Based on their study, they find an interstellar magnetic irregularity scale of order 100 pc. Using this value, we find the total radial distance S from the birthplace of the particles to be approximately 100 pc and 4.5 kpc for the electrons and protons, respectively. In any case, it is clear that the radial distance travelled by the protons is much larger than that by electrons. Likewise, the energy loss lifetime of protons (E/\dot{E}) is much larger than that of the electrons (by a factor of ~ 2000) since it is proportional to the mass of the particles. From these estimates, one expects that the proton bremsstrahlung should play a significant role if bremsstrahlung is responsible for the presence of the hard power law tail in the spectrum. This is due to the longer range and energy loss lifetime of the protons compared to electrons. If indeed the birthplace of the energetic electrons and protons are the sites of supernova explosions in the Galaxy, electron bremsstrahlung will produce localized hard X-ray emission (i.e. hot spots). On the other hand, proton bremsstrahlung will cause the radiation to be smoothly distributed over the Galaxy. This interpretation implies that SNRs play a dominant role in the energetics of ISM via both thermal and non-thermal emission processes.

Finally, we calculate the hydrogen ionization rate for the ISM in this model. If non-thermal bremsstrahlung dominates above 10 keV, then from our model, the average volume emissivity in the 10 – 60 keV for the ridge is $1.9 \times 10^{-29} \text{ erg s}^{-1} \text{ cm}^{-3}$. The average radiation yield in the 10 – 60 keV band is $\sim 10^{-4}$. This yields a collisional loss rate of $1.9 \times 10^{-25} \text{ erg s}^{-1} \text{ cm}^{-3}$. For an average energy loss of 36 eV ($5.8 \times 10^{-11} \text{ erg}$) per hydrogen atom ionized in the ISM (Dalgarno & Griffing 1958), we find an average ionization rate of $3.3 \times 10^{-15} n_H^{-1} (\text{atom s})^{-1}$ for the entire ridge where n_H is the average hydrogen density. Previous values derived from observations have been within $10^{-15} - 10^{-14} (\text{atom s})^{-1}$ (Dalgarno & McCray 1972; Reynolds et al. 1973 from $H\beta$ observations). Our estimate is consistent

with these values for an average $n_H \sim 1 \text{ atom cm}^{-3}$ in the ISM.

Independent of n_H , from the intensity of Galactic $H\alpha$ background at high Galactic latitudes, Reynolds (1984) has derived $(2 - 7) \times 10^6 \text{ s}^{-1}$ hydrogen ionizations (with a “best fit” value of $4 \times 10^6 \text{ s}^{-1}$) per cm^2 column perpendicular to the Galactic disk for the region within $2 - 3 \text{ kpc}$ of the Sun. Our results imply $3.3 \times 10^{-15} \text{ s}^{-1} \text{ cm}^{-3}$ hydrogen ionizations averaged for the ridge. Since in our model, the thickness of the broad disk is $\sim 1 \text{ kpc}$, our results imply hydrogen ionizations of $\sim 9.9 \times 10^6 \text{ s}^{-1} \text{ cm}^{-2}$ of the Galactic disk which is larger than the $H\alpha$ estimate by more than a factor of 2. One reason could be that our estimate is derived by averaging over the central 30° of the plane in longitude where the hard X-ray emission is more intense, while the rate from $H\alpha$ observation is for regions within $2 - 3 \text{ kpc}$ of the Sun. In any case, this indicates that the collisional losses associated with the bremsstrahlung emission from energetic particles to produce the hard X-ray tail are more than adequate to account for the observed hydrogen ionization rate in the ISM.

5. CONCLUSIONS

Our results are summarized as follows: (1) From the *RXTE* survey of the Galactic plane, we find that the diffuse emission from the Galactic ridge has two spatial components: a thin disk of width $\lesssim 0.5^\circ$, and a broad component with a functional form that can be approximated by a Gaussian distribution of about 4° FWHM. Assuming an average distance of 16 kpc to the edge of galaxy, this translates to a height of 70 pc and 500 pc for the thin and broad disk, respectively. (2) A hard power law tail is clearly detected in the spectrum and dominates above 10 keV , implying that the emission in hard X-ray possibly has non-thermal origin. On the other hand, the detection of the emission line from He-like iron in the spectrum (and also lower energy lines from Mg, Si, S in the spectrum from *ASCA*) motivates the idea that part of the emission below 10 keV has thermal origin. (3) The spectrum in the $3 - 35 \text{ keV}$ band can be well modelled with a Raymond-Smith plasma component of $2 - 3 \text{ keV}$ plus a power law component of photon index ~ 1.8 . The spectrum above 10 keV simultaneously fitted with *OSSE*’s spectrum can be fitted with a power law of photon index 2.3 ± 0.2 . The change in the power law slope at lower energies hints at the possibility that the power law either flattens or gradually attenuates below some energy between $10\text{-}100 \text{ keV}$. (5) The characteristics of the thermal component of the diffuse emission resembles that of the SNRs. From this interpretation, we calculate that a SN explosion rate of less than 5 per century is adequate to power the thermal emission from the ridge. (6) The origin of the emission in the hard X-ray band modelled by a power law is uncertain. While unresolved discrete sources are expected to contribute, the bulk of the emission is expected to be of diffuse origin.

One possibility is the non-thermal bremsstrahlung of electrons and protons which may have been accelerated in the SNR sites. Based on the empirical modeling of the data in a wide energy band, we speculate that the power law either flattens or gradually attenuates at lower energies. This lessens the large power injection required to explain the hard power law tail via either electron or proton bremsstrahlung. It will also make it consistent with the power injected to the Galaxy via supernova explosion. (7) The hydrogen ionization rate implied from our model is $3.3 \times 10^{-15} n_H^{-1} (\text{atom s})^{-1}$ averaged over the central ridge. Generally, values of $10^{-15} - 10^{-14} (\text{atom s})^{-1}$ are expected in the ISM. This is an indication that the collisional losses associated with the bremsstrahlung radiation of energetic particles that produce the hard power law tail are sufficient to explain the ionization rates observed in the ISM.

Finally, we expect that simultaneous *RXTE*/*OSSE* observations of the diffuse emission from the Galactic ridge will allow the exclusion of hard discrete sources from the spectrum and will tightly constrain the hard tail slope that dominates in the hard X-ray/soft γ -ray band. This will enhance our understanding of the origin of the power law tail and the energetics of ISM.

We are grateful to Elihu A. Boldt for many valuable discussions, in particular for bringing the process of proton bremsstrahlung to our attention and his contribution to the relevant arguments presented in this paper. We also thank him for a careful reading of the manuscript. We acknowledge G. E. Allen, E. Boldt, K. Ebisawa, S. Hunter, K. Jahoda, G. M. Madejski, R. M. Mushotzky, and R. Petre for useful discussions. We are grateful to J. G. Skibo for providing the diffuse emission spectrum measured with *OSSE*. The help of Pat Tyler and Seth Digel in producing Plate 1 is greatly appreciated. We thank the referee, K. Koyama, for many insightful comments that led to the improvement of this paper. A.V. acknowledges support from the National Academy of Sciences and the National Research Council through a research associateship at NASA's Goddard Space Flight Center.

REFERENCES

- Allen, G. E. et al. 1997, ApJ, 487, L97
- Baring, M. G. 1997, in Very High Energy Phenomena in the Universe, eds. Y. Giraud-Heraud & J. Tran Thanh Van (Editions Frontieres, Paris), 107
- Berger, M. J., & Seltzer, S. M. 1964, NASA publication # SP-3012
- Barkas, W. H., & Berger, M. J. 1964, NASA publication # SP-3013
- Bleach, R. D., Boldt, E. A., Holt, S. S., Schwartz, D. A., & Serlemitsos, P. J. 1972, ApJ, 174, L101
- Boldt, E., & Serlemitsos, P. 1969, ApJ, 157, 557
- Dalgarno, A. & Griffing, G. W. 1958, Proc. Roy. Soc. London, A. 250, 426
- Dalgarno, A., & McCray, R. A. 1972, A.R.A.A., vol. 10, 375
- Green, D. A. 1996, 'A Catalogue of Galactic Supernova Remnants (1996 August Version)', Mullard Radio Astronomical Observatory, Cambridge, UK (available on the WWW at <http://www.mrao.cam.ac.uk/survey/snr/>).
- Helfand, D. J., Velusamy, T., Becker, R. H., & Lockman, F. J. 1989, ApJ, 341, 151
- Iwan, D., Marshall, F. E., Boldt, E. A., Mushotzky, R. F., Shafer, R. A., & Stottlemeyer, A. 1982, ApJ, 260, 111
- Jahoda, K., Swank, J. H., Giles, A. B., Stark, M. J., Strohmayer, T., Zhang, W., & Morgan, E. H. 1996, Proc. SPIE, 2808, 59
- Kaneda, H. 1997, Ph.D. Dissertation, University of Tokyo
- Kaneda, H., Makishima, K., Yamauchi, S., Koyama, K., Matsuzaki, K., & Yamasaki, N. Y. 1997, ApJ, 491, 638
- Kim, K.-T., P. P. Kronberg, & Landecker, T. L. 1988, AJ, 96, 704
- Koyama, K., Ikeuchi, S., & Tomisaka, K. 1986, PASJ, 38, 503
- Koyama, K., Makishima, K., Tanaka, Y., & Tsunemi, H. 1986, PASJ, 38, 121
- Koyama, K., Petre, R., Gotthelf, E. V., Hwang, U., Matsuura, M., Ozaki, M., & Holt, S. S. 1995, Nature, 378, 255

- Koyama, K., Kinugasa, K., Matsuzaki, K., Nishiuchi, M., Sugizaki, M., Torii, K., Yamauchi, S., & Aschenbach, B. 1997, PASJ, 49, L7
- Lagage, P. O., & Cesarsky, C. 1983, J. Astron. & Astrophys. 125, 249
- Levine, A. M., et al. 1984, ApJS, 54, 581
- Milne, D. K. 1979, Australian J. Phys., 32, 83
- Ottmann, R., & Schmitt, J. H. M. M. 1992, A&A, 256, 421
- Patterson, J. 1984, ApJS, 54, 443
- Pohl, M., Kanbach, G., Hunter, S. D., & Jones, B. B. 1997, ApJ, 491, 159
- Purcell, W. R. et al. 1996, A&AS, 120, 389
- Raymond, J. C., Cox, D. P., & Smith, B. W. 1976, ApJ, 204, 290
- Reynolds, R. J., Roesler, F. L., Scherb, F. 1973, ApJ, 179, 651
- Reynolds, R. J. 1984, ApJ, 282, 191
- Sedov, L. I. 1959, Similarity and Dimensional Methods in Mechanics (Academic Press, New York)
- Schlickeiser, R. 1997, A&A, 319, L5
- Skibo, J. G., Ramaty, R., & Purcell, W. R. 1996, A&AS, 120, 403
- Skibo, J. G. et al. 1997, ApJ, 483, L95
- Spitzer, L., Jr., 1968, Diffuse Matter in Space (Interscience Publisher, New York)
- Tammann, G. A. 1982, in Supernovae: A Survey of Current Research, ed. M. J. Rees and R. J. Stoneham, 371
- The, L. S. et al. 1995, ApJ, 444, 244
- Tomisaka, K., Habe, A., & Ikeuchi, S. 1980, Prog. Theor. Phys., 64, 1587
- Townes, C. H. 1989, in IAU Symp. 136, The Center of the Galaxy, ed. M. Morris (Dordrecht,: Kluwer), 1
- Warwick, R. S., Turner, M. J. L., Watson, M. G., & Willingale, R. 1985, Nature, 317, 218

- Worrall, D. M., Marshall, F. E., Boldt, E. A., & Swank, J. H. 1982, *ApJ*, 255, 111
- Yamasaki, N. 1996, Ph.D. Dissertation, University of Tokyo
- Yamasaki N. Y. et al. 1997, *ApJ*, 481, 821
- Yamauchi et al. 1996, *PASJ*, 48, L15
- Yamauchi, S., Koyama, K., Kinugasa, K., Torii, K., Nishiuchi, M., Kosuga, T., Kamata, Y.
1998, *Astronomische Nachrichten*, vol. 319, no. 1, 111

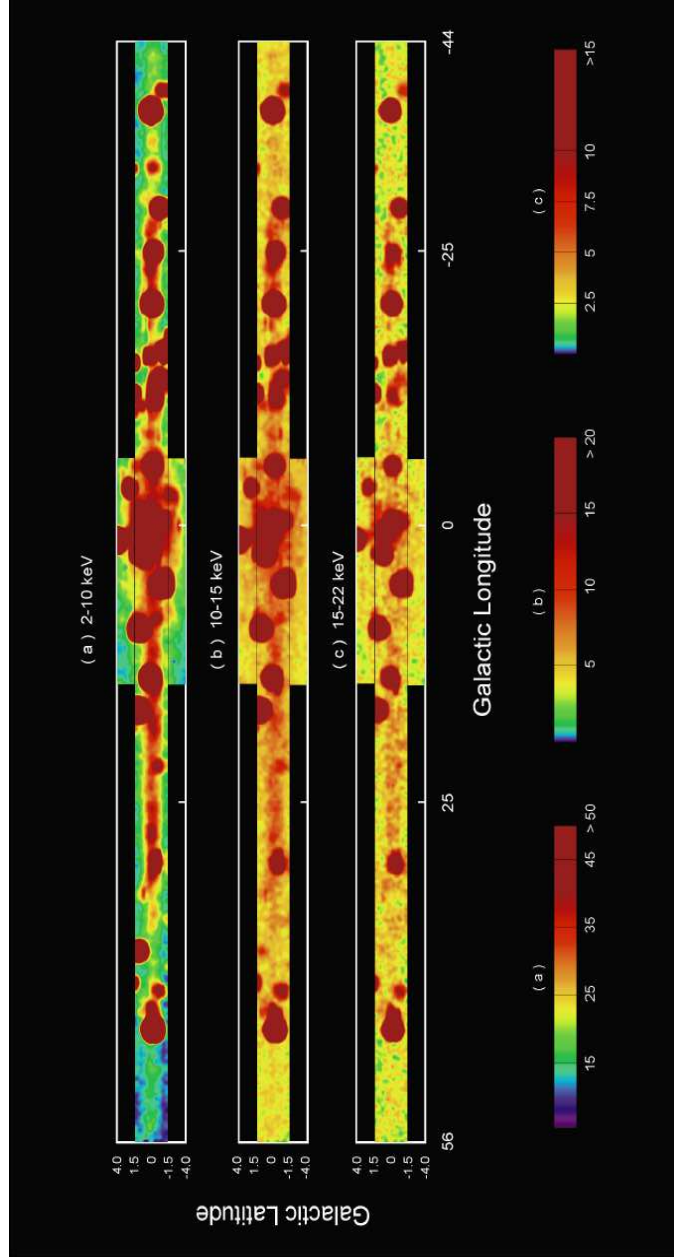


Fig. 1.— Maps of the Galactic ridge X-ray emission for 3 energy bands of (a) 2 – 10 keV, (b) 10 – 15 keV, and (c) 15 – 22 keV. Color bars corresponding to each map appear at the bottom. See §2 for details. **Note:** A high quality tiff image of this color plate can be obtained via anonymous ftp to <ftp://lheaftp.gsfc.nasa.gov/local/LHEA/FTP/pub/valinia/ridge/ridge.tiff>. For a hard copy, write to Azita Valinia at valinia@milkyway.gsfc.nasa.gov.

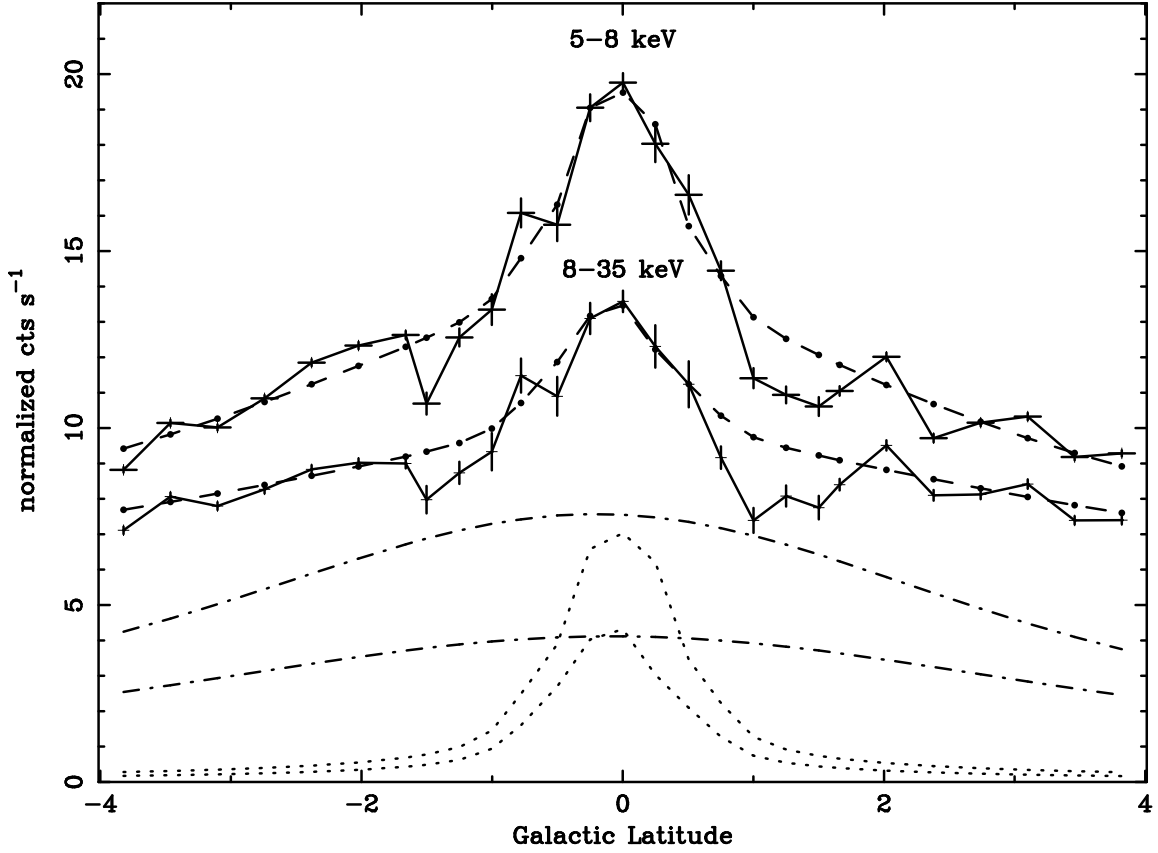
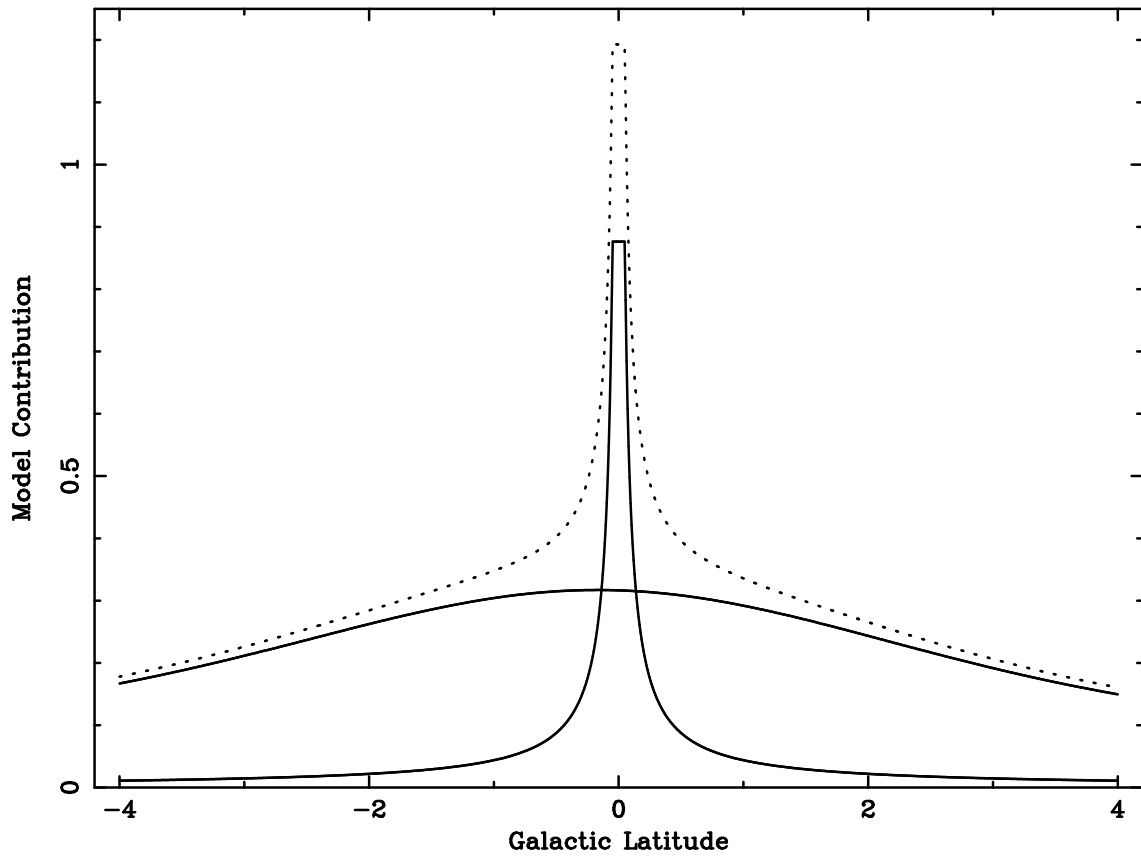


Fig. 2.— (a) (this page) Latitude Distribution of the diffuse emission averaged over $-15^\circ < l < 15^\circ$ for the 5 – 8 keV and 8 – 35 keV energy bands (solid curves). Position of the error bars show the measured averaged count rate at that latitude. Dashed curves represent the results of the convolution of a thin plus broad spatial model to the detector’s response function. Dotted and dash-dot curves show the convolution of the thin disk and broad models, respectively (5 – 8 keV: upper curves; 8 – 35 keV: lower curves). A constant component (not shown) is included in the model to account for the cosmic X-ray background. See §3.3 for parameters of the fit. (b) (next page) Contribution of the thin and broad spatial components to the 5-8 keV flux as a function of Galactic latitude in arbitrary units. Dotted curve shows the combined contribution of both components.



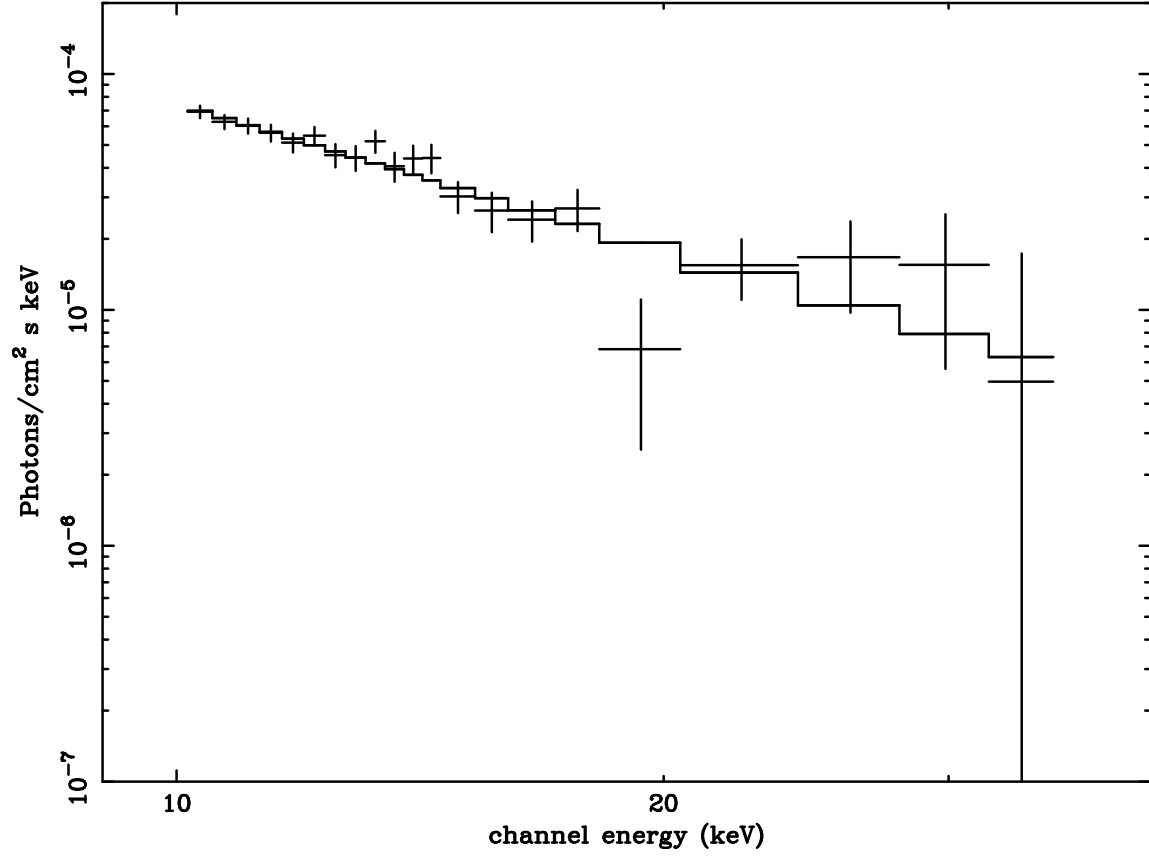


Fig. 3.— Unfolded spectrum and best fit model (power law) for the central region of the ridge (R1) in the 10 – 35 keV band.

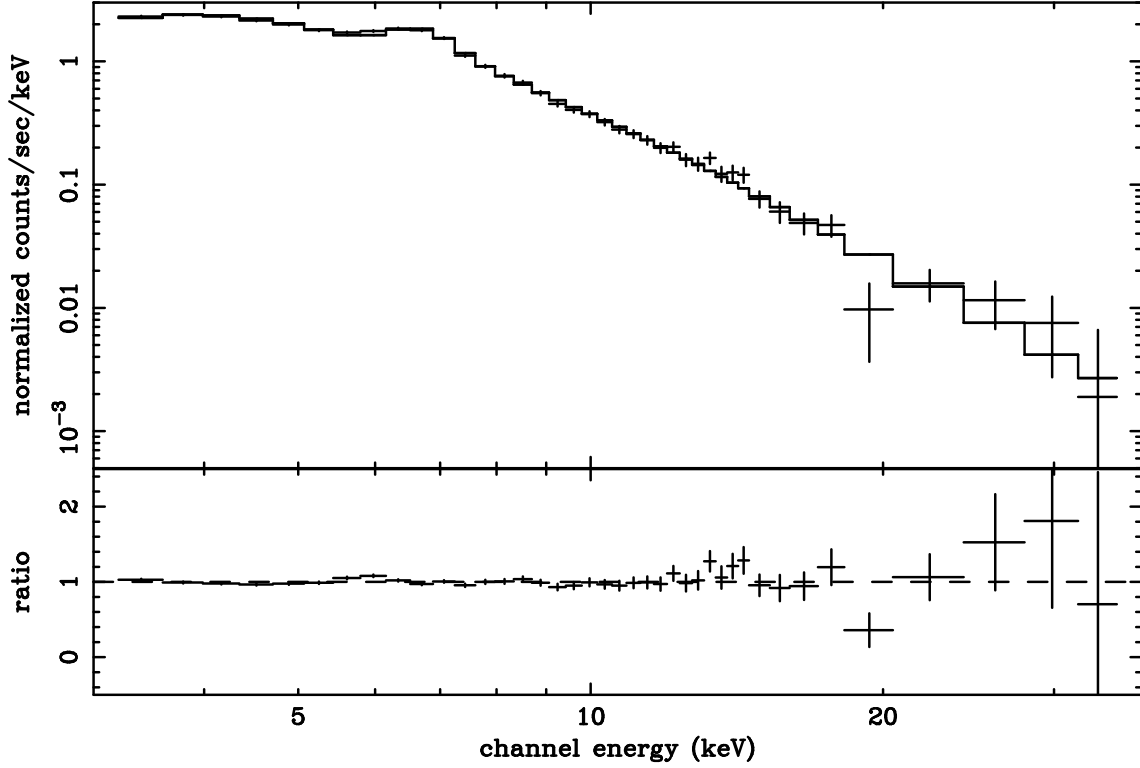
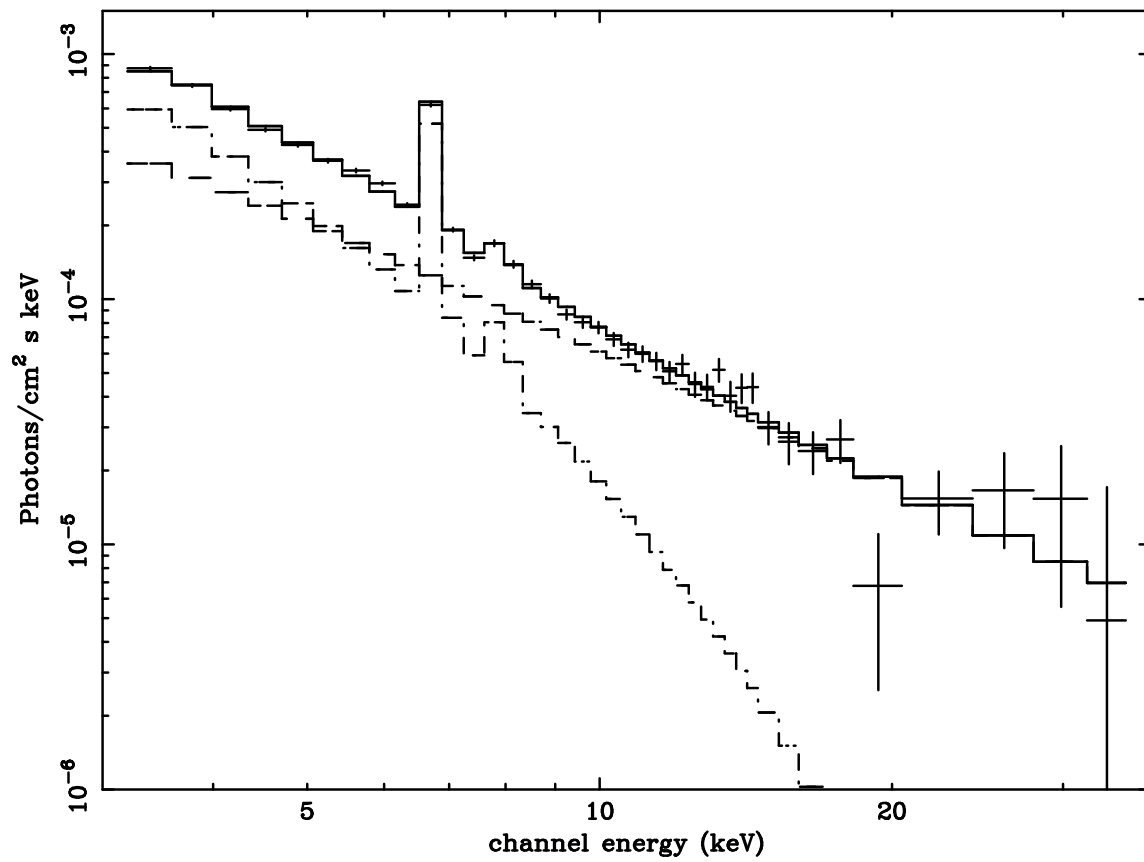


Fig. 4.— Results of modeling the spectrum from the central region of the ridge (R1) in the 3 – 35 keV energy band (see Table 3 for model parameters): (a) (this page) Data and folded model (b) (next page) Unfolded spectrum and model. Contributions to the model from various components are also shown.



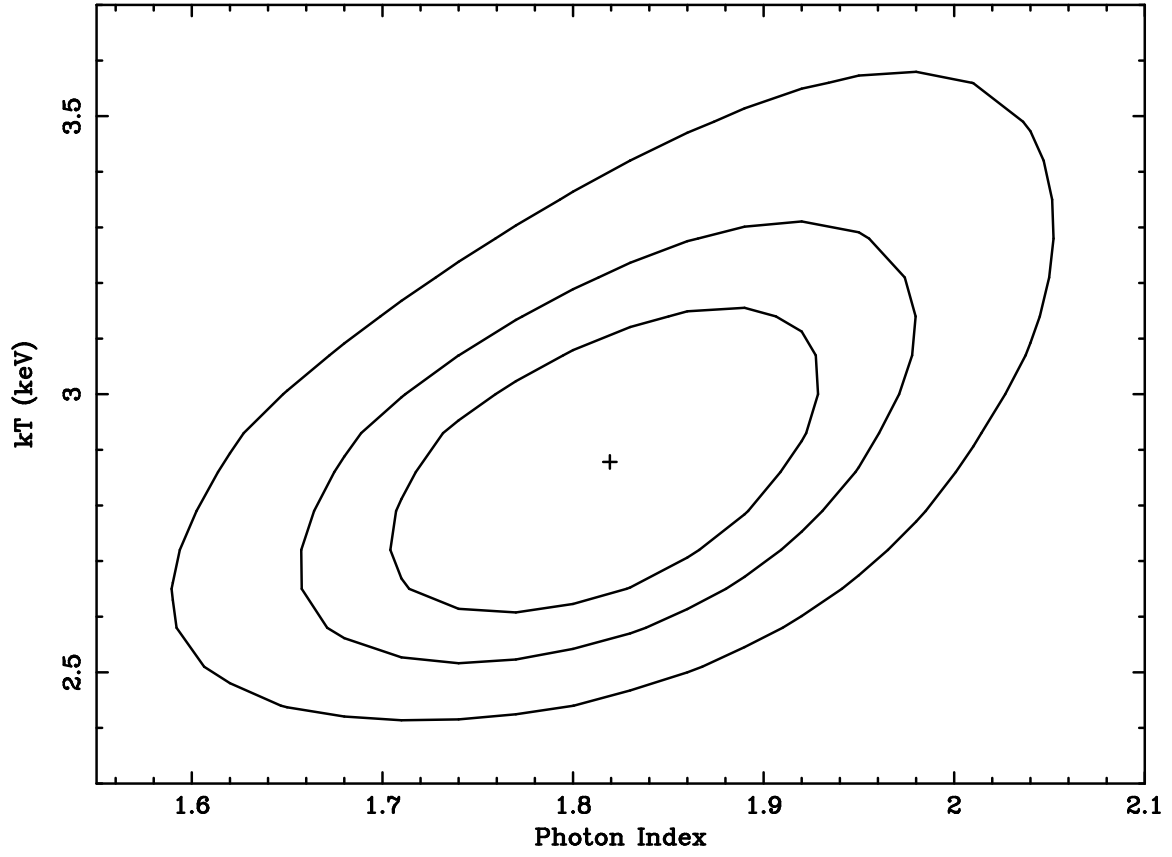


Fig. 5.— Confidence contour plot of Raymond-Smith plasma temperature vs. power law photon index for the model presented in Table 3 and Figure 4.

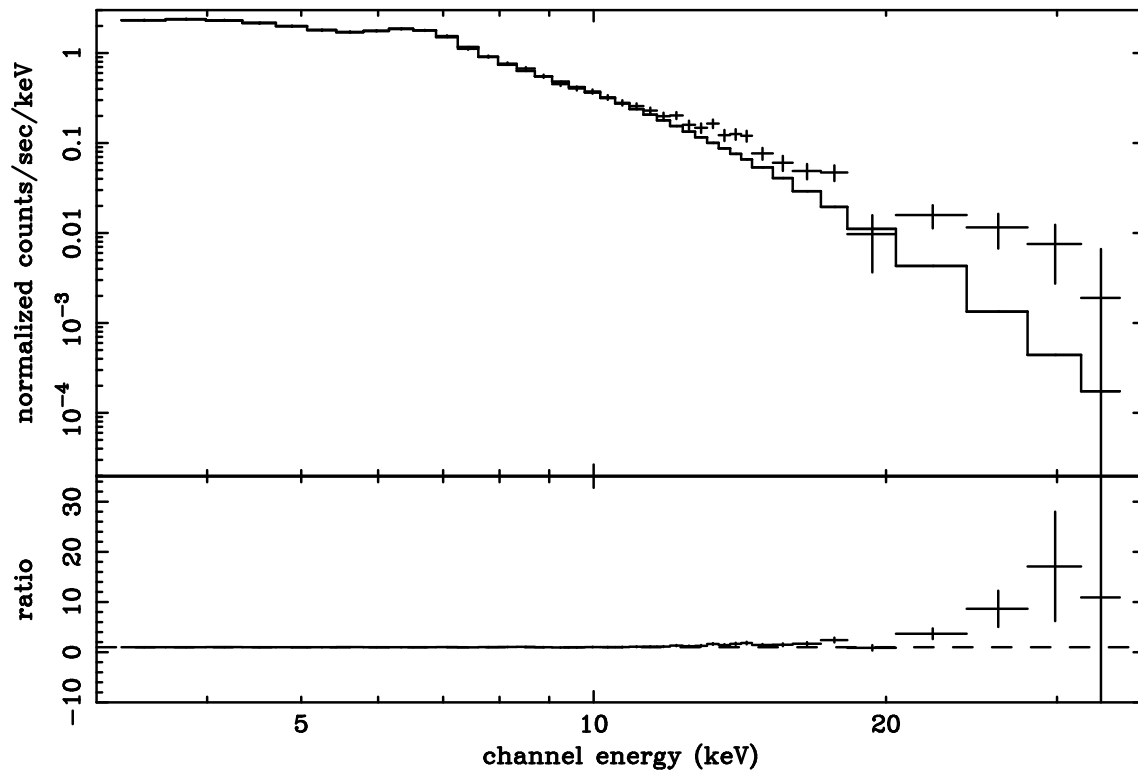


Fig. 6.— RXTE data in the 3-35 keV band folded with the best fit model derived from analysis of ASCA data in the 2 – 10 keV band (Kaneda et al. 1997).

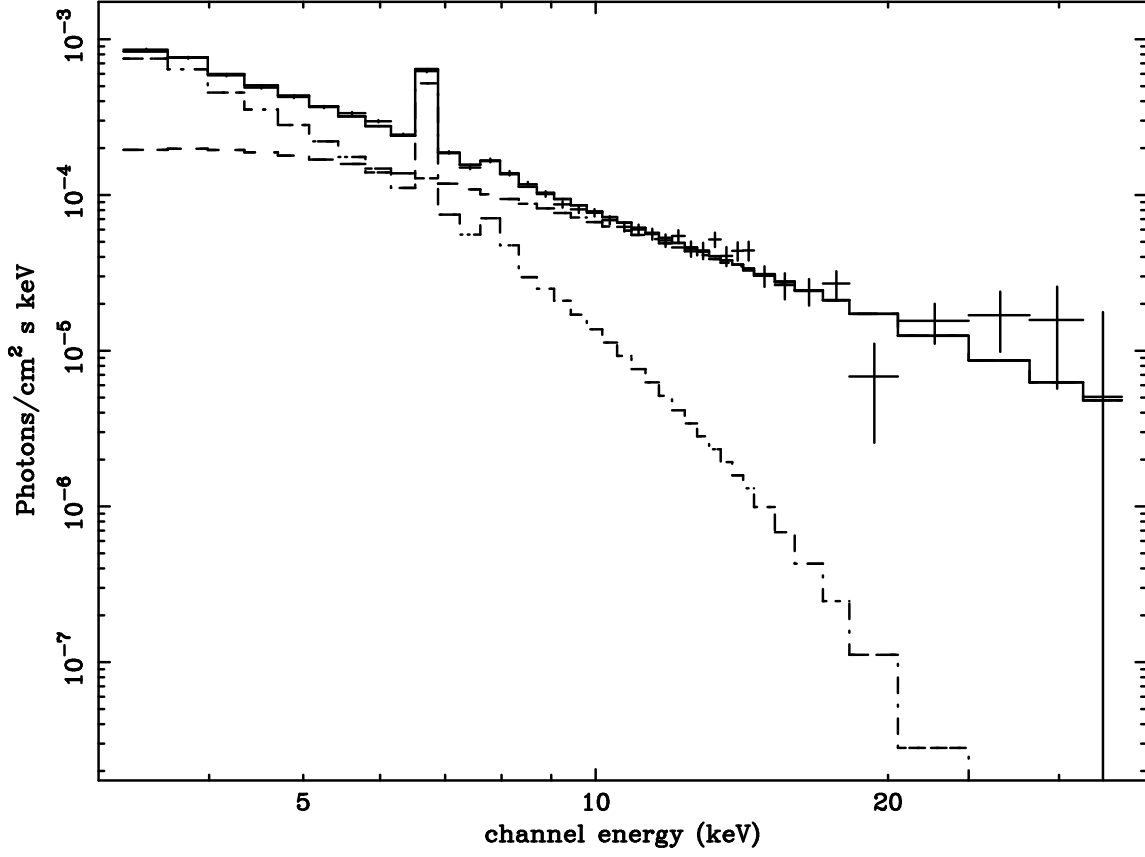


Fig. 7.— Unfolded spectrum and model (presented in Table 4) for the central ridge (R1). The power law is multiplied by an exponentially absorbing function to mimic the flattening of the power law at lower energies.

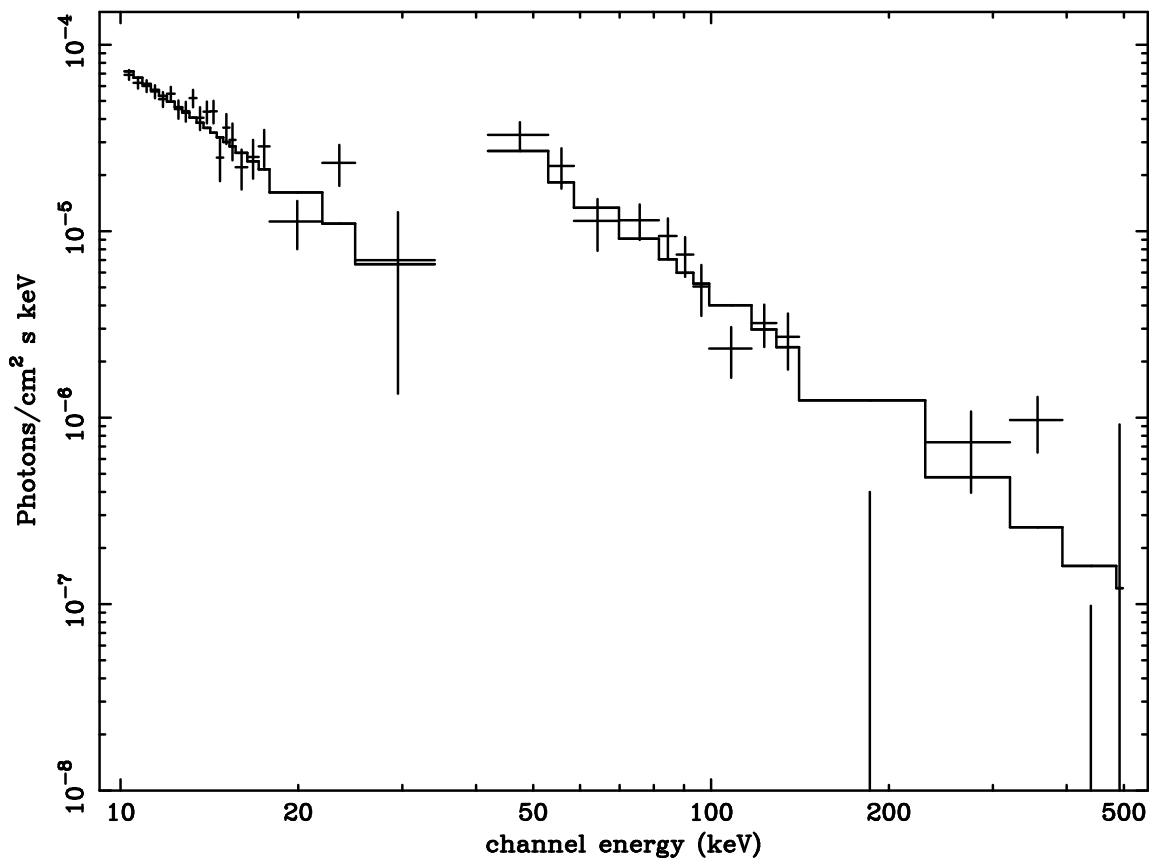


Fig. 8.— Simultaneous fit to the diffuse emission spectra from $l = 95^\circ$ obtained with *OSSE*, and the central region of the ridge (R1) obtained with *RXTE*. See §3.6 for details.

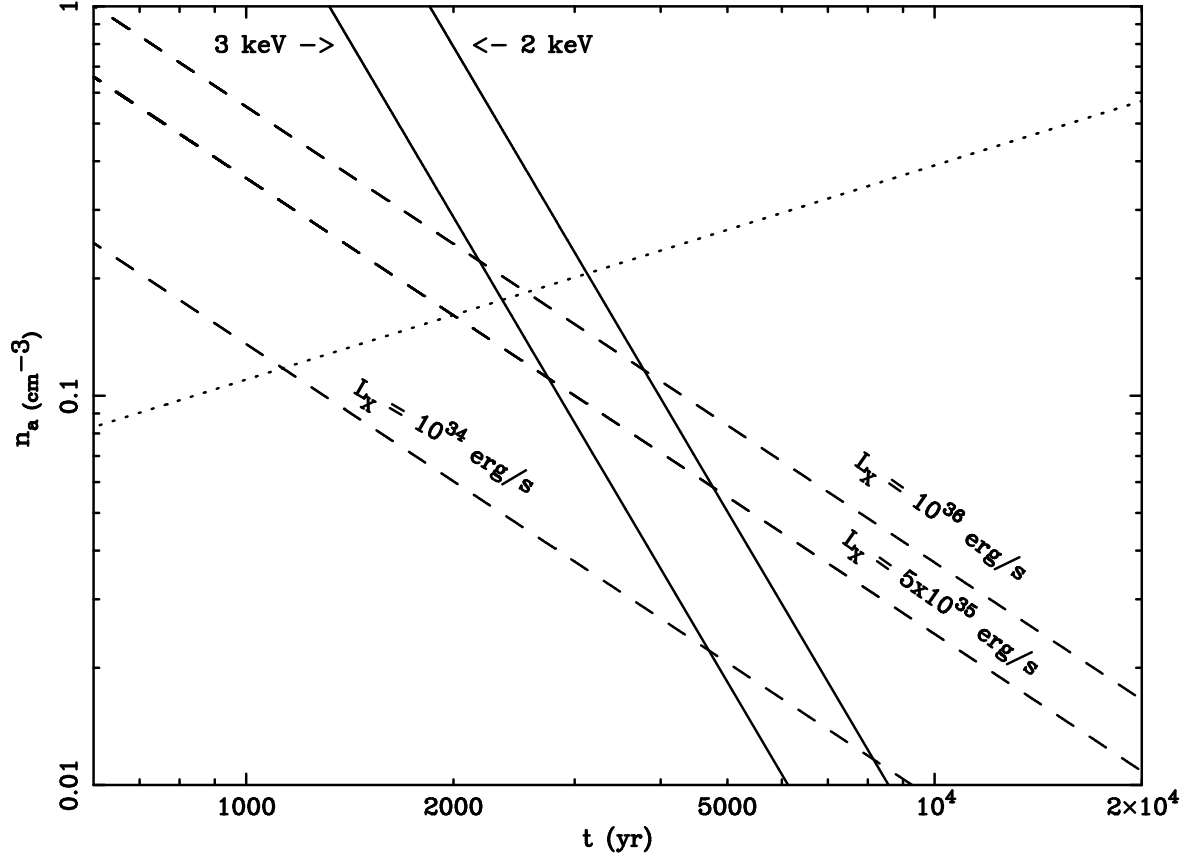


Fig. 9.— Constraints on the blast wave temperature (solid lines) and SNR detectability in radio (dotted line) are plotted in the ambient density-SNR age phase space. Dotted line gives the condition of the surface brightness of the remnant to be $10^{-20} \text{ W m}^{-2} \text{ Hz}^{-1} \text{ sr}^{-1}$ (eq. [3]). Constant luminosity lines (dashed lines) are also plotted. The allowable zone from the argument given in the text is confined to the space between the two solid lines and below the dotted line.

Table 1. Detected Sources in the RXTE Scans of the Galactic Ridge

Source	l	b
J1744-28	0.044	0.301
GRS1739-278	0.660	1.167
SL1735-269	0.785	2.400
K1731-260	1.074	3.655
4U1744-26	2.294	0.793
GX5-1	5.079	-1.018
4U1745-203	7.725	3.795
GX9+1	9.072	1.154
GX13+1	13.518	0.108
GX17+2	16.432	1.276
4U1812-12	18.033	2.362
G21.5-0.9	21.493	-0.887
GR11(1)	22.001	-0.002
EXO1846-031	29.954	-0.917
G1843+009	33.108	1.746
GPS1858+015	35.416	-1.648
XTE J1856+053*	38.258	1.266
EXO1902+054	39.33	-0.390
SS433	39.695	-2.247
4U1909+07	42.089	-0.940
W49B	43.275	-0.189
A1907+09	43.743	0.477
GRS1915+105	45.366	-0.219
MSH15-52	320.321	-1.161
CIRCINUSX-1	322.117	0.038
4U1553-542	327.945	-0.857
2E1614-505	332.421	-0.422
1608-522	330.926	-0.850
4U1624-49	334.914	-0.263
GX340+0	339.587	-0.079
2S1702-429	343.887	-1.314
OAO1653-40	344.369	0.326
NSCO94	344.982	2.456
4U1708-408	346.327	-0.928

Table 1—Continued

Source	l	b
GPS1709-396	347.300	-0.333
4U1700-37	347.755	2.173
GPS1713-388	348.394	-0.543
CTB37A/B	348.598	0.232
GX349+2	349.105	2.750
EXO1722-363	351.474	-0.548
A1744-361	354.121	-4.192
MXB1728-34	354.305	-0.151
X1730-333	354.843	-0.159
TERZAN2	356.320	2.298
SL1746-331	356.816	-2.997
H1741-322	357.125	-1.607
R1747-313	358.556	-2.168
2S1742-294	359.559	-0.390
A1742-289	359.930	-0.043

*Previously unknown source discovered with RXTE. See IAUC 6504

Table 2. Spatial Divisions of the Galactic Ridge

Region	Galactic Longitude	Galactic Latitude	Exposure Time (ks)
R1	$-45^\circ < l < 45^\circ$	$-1^\circ.5 < b < 1^\circ.5$	21.5
R2	$-15^\circ < l < 15^\circ$	$1^\circ.5 < b < 4^\circ.0$	12.5
R3	$-15^\circ < l < 15^\circ$	$-4^\circ.0 < b < -1^\circ.5$	13.1

Table 3. Best fit model parameters for the 3 – 35 keV spectrum from region R1

Model Component	Parameter	Value
Absorption ^a Raymond-Smith	N_H (10^{22} cm ⁻²)	$1.8^{+0.6}_{-0.4}$
	kT (keV)	2.9 ± 0.3
	Abundance (Solar) ^b	1.0
	Normalization ^c	1.8×10^{-5}
Power Law	Photon Index	1.8 ± 0.1
	Normalization ^c	6.2×10^{-5}
	$\chi^2/\nu = 115.4/60 = 1.9$	

^aAbsorption of CXB spectrum by Galactic disk has also been taken into account. See §3.4.2 for details.

^bFrozen

^cUnabsorbed flux (photon s⁻¹ cm⁻² keV⁻¹) at 10 keV

Table 4. Same as Table 3 except that the power law is multiplied by an exponentially absorbing function $M(E) = \exp(E/E_0)$

Model Component	Parameter	Value
Absorption ^a Raymond-Smith	N_H (10^{22} cm ⁻²)	$2.0^{+1.6}_{-0.6}$
	kT (keV)	2.3 ± 0.4
	Abundance (Solar) ^b	1.0
	Normalization ^c	1.4×10^{-5}
Power Law	Photon Index	$2.7^{+1.2}_{-0.7}$
	E_0	$8.5^{+7.9}_{-6.5}$
	Normalization ^c	6.8×10^{-5}
	$\chi^2/\nu = 112.2/59 = 1.9$	

^aAbsorption of CXB spectrum by Galactic disk has also been taken into account. See §3.4.2 for details.

^bFrozen

^cUnabsorbed flux (photon s⁻¹ cm⁻² keV⁻¹) at 10 keV

Table 5. Best fit model parameters for the 3 – 35 keV spectrum from region R2

Model Component	Parameter	Value
Absorption ^a Raymond-Smith	N_H (10^{22} cm^{-2})	$0.2^{+0.7}_{-0.2}$
	kT (keV)	$3.4^{+0.4}_{-0.6}$
	Abundance (Solar) ^b	1.0
	Normalization ^c	1.6×10^{-5}
Power Law	Photon Index	1.7 ± 0.2
	Normalization ^c	4.9×10^{-5}
$\chi^2/\nu = 71.2/60 = 1.2$		

^aAbsorption of CXB spectrum by Galactic disk has also been taken into account. See §3.4.2 for details.

^bFrozen

^cUnabsorbed flux ($\text{photon s}^{-1} \text{ cm}^{-2} \text{ keV}^{-1}$) at 10 keV

Table 6. Best fit model parameters for the 3 – 35 keV spectrum from region R3

Model Component	Parameter	Value
Absorption ^a Raymond-Smith	N_H (10^{22} cm^{-2})	$0.1^{+0.6}_{-0.1}$
	kT (keV)	$3.9^{+0.9}_{-0.7}$
	Abundance (Solar) ^b	1.0
	Normalization ^b	2.3×10^{-5}
Power Law	Photon Index	$1.8^{+0.3}_{-0.1}$
	Normalization ^c	5.0×10^{-5}
$\chi^2/\nu = 80.4/60 = 1.3$		

^aAbsorption of CXB spectrum by Galactic disk has also been taken into account. See §3.4.2 for details.

^bFrozen

^cUnabsorbed flux ($\text{photon s}^{-1} \text{ cm}^{-2} \text{ keV}^{-1}$) at 10 keV